Description of downscaling methodologies
Deliverable D3.3

Edited by: Roberto Aurelio Chávez Arroyo
Delivery date: 22 April 2016
Dissemination level: Public

With financial support from NEWA ERA-NET Plus, topic FP7-ENERGY.2013.10.1.2.

Author Information

Name	Organisation	E-mail
Roberto Chávez Arroyo	CENER	rchavez@cener.com
Javier Sanz Rodrigo	CENER	jsrodrigo@cener.com
Andreas Bechman	DTU	
Matias Avila	BSC	
Herbert Owen	BSC	
Chi-Yao Chang	IWES	
Arnaud Candaele	CENAERO	

Table of Contents

Executive Summary

This report describes the first tasks towards the downscaling methodologies that will be used to link mesoscale outputs from the New European Wind Atlas with microscale models in connection to wind farm design tools.

This initial report provides a review of existing downscaling methodologies applied in the context of wind energy applications. This is used to frame the development of the NEWA model-chain which will allow microscale models to be used in connection to input data derived from mesoscale models. The mesoscale to microscale methodology will provide means to relate the long-term wind climatology, characterized by a mesoscale model, with the design conditions at site level where wind farm design takes place.

This report deals with microscale models, typically implemented on computational fluid dynamic (CFD) solvers. A list of the participating models in NEWA is provided in the Annex. The initial challenge is to make theses codes intercomparable so we can extract meaningful conclusions when we evaluate simulations in connection with validation cases. Before comparing simulations and observational data, we need to assess the numerical error due to the sensitivity of the result to the model set-up. This is particularly important in complex terrain where grid dependencies can be significant.

The objective of the initial effort of the NEWA microscale team has been focused on using different methods of assessing grid dependencies. This has been done with different microscale models applied to the three complex terrain test cases where dedicated field experiments are planned: Kassel (forested hill), Perdigao (double-hill) and Alaiz (hill and mountain range). In order to make the results more comparable in terms of numerical errors, the reference physical model adopted in the study has been based on neutral, steady-state, surface-layer conditions. This is a Reynolds-independent model that removes the dependency of the results with the wind speed.

The results show significant variability of numerical errors with the grid set-up which includes the inherent sensitivity to the wind direction. These results will be used to define best practices for setting up a microscale model simulation with specific requirements for wind resource assessment applications.

Introduction

A wind atlas is associated to the planning phase of wind energy development, which can last several years from strategic spatial planning, to site prospecting, to wind farm design and financing. Detailed and robust information about the relative size of the wind resource across an area is crucial for the commercial evaluation of a wind farm.

Today a number of well-established models and methodologies exist for estimating resources and design parameters. These can work well if good local data are available, but the wind energy community is still hampered by projects having large negative discrepancies between calculated and actual resources and design conditions.

Since the late 80's, the de facto standard model for wind assessment has been WAsP which estimates the effect of the micro-scale (0.05-5 km scale) terrain and vegetation variations on the wind resource (Troen and Petersen, 1989). As wind turbines have grown, such a micro-scale approach needs to be complemented with the modelling of the planetary boundary layer (PBL) and associated temperature gradients within the PBL (Petersen and Troen, 2012). Whereas the micro-scale flow models can be seen as bottom-up approaches for wind resource assessments over a smaller area, the use of meso-scale models has since the 1990ies offered a top-down approach to wind resource estimations over large areas to produce wind atlases. However, the meso-scale models cannot accurately predict the wind variability caused by micro-scale features. The main question is how to make these two approaches, top-down and bottom-up, consistent so that there is a clear understanding about when to switch from one to the other and how to best use both in combination.

A main objective of the NEWA project is to fundamentally change the state-of-the-art during the course of the project by developing and introducing a new methodology for the assessment of wind conditions based on a mesoscale to microscale model-chain approach. A generally approved method is highly needed so that data generated by the mesoscale model can be adapted and collated for use in various microscale models. Such method will be validated in various terrain and wind climate conditions considering dedicated experiments in NEWA.

1. Wind Atlas Scope

The New European Wind Atlas will provide a unified high-resolution and freely available dataset of wind resource in Europe. Wind statistics will cover onshore Europe and 100 km offshore plus the Baltic and the North Seas (Figure 1), with a horizontal resolution of 20-30 meters at least at 10 wind turbine relevant heights. The database will be based on at least 10 years of mesoscale simulations at 3 km resolution, with long-term corrections as well as subgrid microscale corrections to reduce the bias on the local mean wind resource.

In addition to wind resource information, the new wind atlas will provide information about site suitability conditions (turbulence intensity, wind shear, extreme wind speed), wind variability as well as and wind power predictability from day-ahead to decadal. A

probabilistic wind atlas methodology using mesoscale models is introduced in D3.1, and methodologies for predictability assessment are introduced in D3.2.

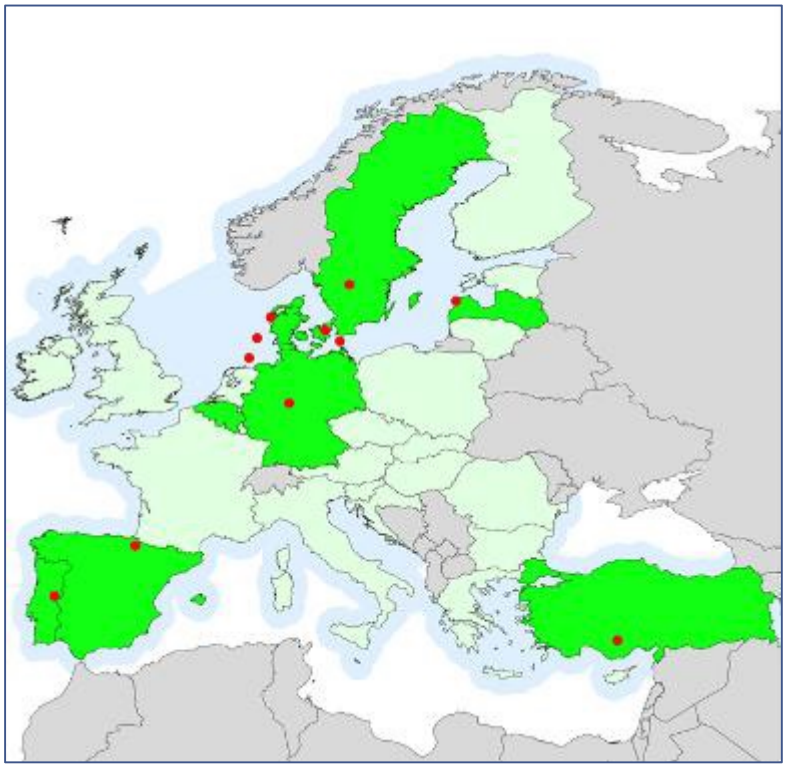

Figure 1: Initial extension of the European domain for the New European Wind Atlas and location of high fidelity experiments

Besides variables of immediate use by resource planners, the wind atlas will provide means to feed boundary conditions on microscale models. This will allow not only to improve the wind atlas predictions at local level when better site data becomes available but also to allow a coherent integration with wind farm design tools. Hence, a generalized wind atlas, i.e. free of site effects, will be also part of the NEWA database.

Integral to the wind atlas methodology is the assessment of the associated uncertainties. The ultimate goal of the wind atlas is to reduce the uncertainties on the assessment of wind resource and the wind conditions that affect the design of wind turbines. To this end, the model-chain will be thoroughly validated across Europe with dedicated experiments and historical wind resource assessment campaigns from industry. The model evaluation strategy is described in D3.4.

An uncertainty map will calculate the confidence of the wind atlas and, therefore, the intensity to which in situ measurement must be employed before development of a wind farm.

2. Microscale Modelling for Wind Energy Applications

Figure 2 shows schematically the wind assessment model-chain framework with typical scale ranges for each sub-model level and associated applications and flow modeling approaches of various physical fidelity levels (Sanz Rodrigo et al, 2016).

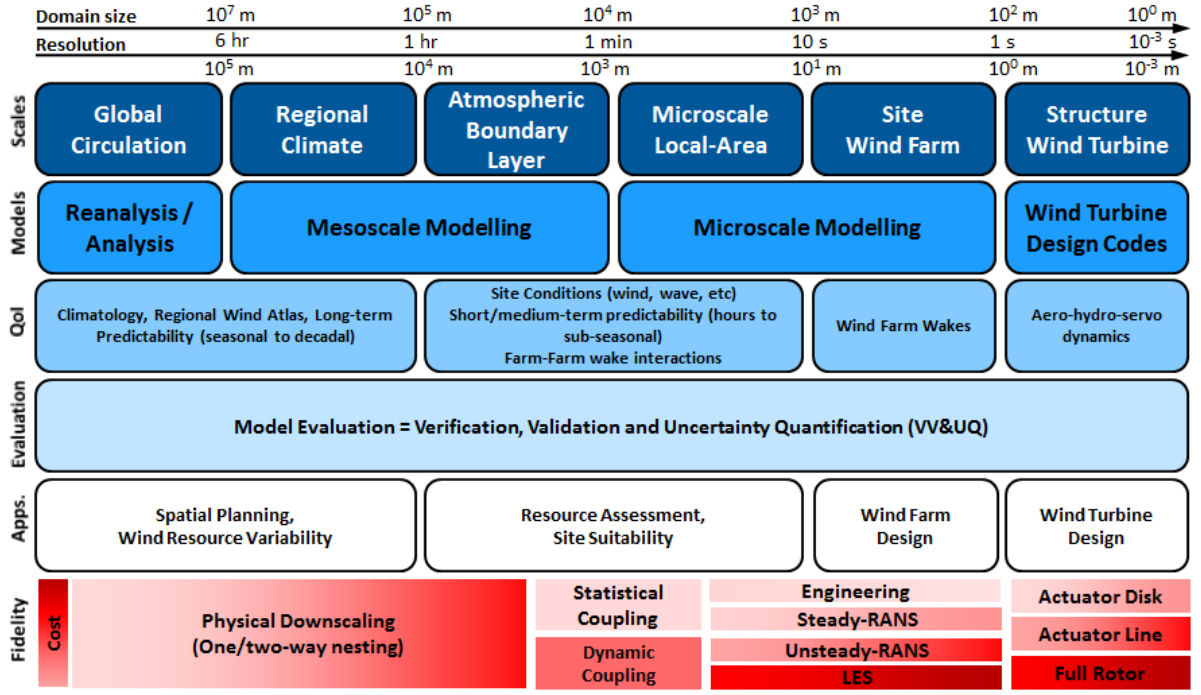

Figure 2: Wind assessment modelling framework indicating typical model scale ranges, relevant quantities of interest for different applications and high-level fidelity levels (the shading indicates the computational cost). (Sanz Rodrigo et al., 2016)

The microscale range is the design space for wind energy developers which comprise the wind farm layout, the turbine characteristics and the topographical site conditions relevant to drive the local wind flow, typically extending 10-20 kilometers horizontally. The increasing size of wind turbines, with rotors already spanning more than 150 m diameter and hub heights above 100 m, requires proper modelling of the atmospheric boundary layer (ABL) from the surface to the free atmosphere. The modeling scope of NEWA, with focus on wind resource, will not include wake modeling so this is left out of this state-of-the-art description.

Since the late 1980's with the appearance of the European Wind Atlas (Troen and Petersen, 1989), the most widely used methodology for wind resource assessment has been WAsP (Wind Atlas Analysis and Application Program). The flow model is based on a linearization of the Navier Stokes equations, a concept that was originally introduced by Jackson and Hunt (1975). Linearized flow models can be used reliably over sufficiently gentle slopes (say below 20%) to ensure fully attached flows (Petersen and Troen, 2012). The WAsP methodology uses simplified diagnostic models to evaluate the local influences of terrain, roughness and obstacles on the met mast wind climatology. Then, it is possible to generate a generalized wind climate of a larger area by removing these

effects (bottom-up or upscaling). Using the same methodology in reverse direction (up-bottom) it is possible to introduce local effects at the target site assuming that the generalized wind climate is shared with the reference site. This assumption depends on how much the generalized climate is modified by regional mesoscale processes between the reference and the target sites. Large mesoscale activity will require shorter distances between reference and target sites in order to apply the generalized wind climate concept (Petersen and Troen, 2012).

In a model-chain context, the wind flow can be considered as the sum of a background ABL in horizontally homogeneous conditions (same concept as the generalized wind climate in WAsP) driven by mesoscale and larger-scale atmospheric processes and locally modified due to flow disturbances from terrain, vegetation, wind turbine wakes, etc. In idealized conditions, we neglect mesoscale tendencies so that the variation of scalar and vector quantities between the surface and the free-atmosphere boundary conditions is the result of the equilibrium among turbulent diffusion, Coriolis forces and horizontal pressure gradients. Assuming equilibrium of the last two in the free-atmosphere, we can relate pressure gradients with a geostrophic wind speed which provides the vertical distribution of horizontal pressure gradient forcing or, alternatively, is used as top boundary condition for the horizontal momentum equations. A barotropic atmosphere (density is only a function of pressure) is often assumed, which neglects variations of the geostrophic wind with height due to horizontal temperature differences ("thermal wind" or baroclinicity). The Boussinesq approximation assumes that density differences can be neglected (incompressible flow) except in the buoyancy term of the vertical component of the momentum equation. Hence, temperature and density vary linearly through the ideal gas law.

These idealized conditions have been used in the past to develop microscale models for the ABL to link surface-layer properties with the free-atmosphere. The turbulent structure of the ABL is simulated with different fidelity levels, from semi-empirical parameterizations typically based on the mixing-length concept (Holt and Raman, 1988), to isotropic eddy-viscosity formulations with one (Weng and Taylor, 2003) or two (Sogachev et al., 2012) Reynolds-averaged Navier Stokes (RANS) equations, to anisotropic RANS equations for the Reynolds stress components (Gibson and Launder, 1978), to Large-eddy simulation (LES) turbulence models that explicitely resolve the turbulence scales of the energy-containing eddies and parameterize the sudbrid turbulence (Beare et al., 2006) to hybrid RANS/LES approaches (Bechmann and Sørensen, 2010). A blind test of models around the Bolund hill with steep terrain in the prevailing wind direction highlighted the differences between a range of fidelity levels (Berg et al., 2011, Bechmann et al., 2011). RANS models, all based on similar physical models, presented the best results overall but showed a large spread mostly due to grid dependencies. LES models, probably not very mature, straggled to deal with such complex geometry and could not provide better results than RANS models on the mean flow. A more recent simulation from Diebold et al. (2013) using the immersed boundary method with LES produced much better results overall with largest deviations near the ground, indicating needs for further research on wall models.

RANS models, built on Computational Fluid Dynamic (CFD) solvers, have become an alternative to linearized models in complex flow environments, as a good compromise

between physical fidelity and computational cost. The application of CFD in wind assessment is still largely based on steady-state RANS turbulence models based on neutral and surface-layer approximations (Palma et al., 2008). Unsteady RANS models are being introduced to simulate the mean flow of the ABL with thermal stratification (Sogachev et al., 2012; Koblitz et al. 2012). LES-based methods are far more costly but provide means to simulate the meandering of the wind field in the presence of terrain (Silva et al., 2007; Bechmann and Sørensen, 2010; Diebold et al., 2013) and be used as high-fidelity models to design reduced-order models. Regardless of the complexity of the turbulence model, they all assume idealized microscale conditions where mesoscale tendencies are not incorporated as additional forcing in the computational domain.

Conventionally, Monin-Obukhov similarity theory (MOST) is used as surface-layer scheme to relate surface properties with the turbulent fluxes in the near-wall cells (Richards and Hoxey, 1993).

Consistent with the background wind profile concept, inflow boundary conditions in CFD-type of models are typically defined in terms of idealized horizontally-homogeneous profiles. Sector-wise, they are defined in terms of the upstream large-scale surface characteristics and calibrated to obtain the target velocity and wind direction at the reference site. Transition from the idealized flat inflow to the real terrain topography is done making use of a buffer region that should be far enough from the area of interest to minimize the impact on the flow at the target sites (Koblitz, 2013). The inflow is generated using MOST analytical profiles in connection to surface-layer models or with precursor ABL simulations using RANS single-column models (Koblitz, 2013), or using an empty 3D domain and periodic inflow-outflow conditions in LES simulations (Bechmann and Sørensen, 2010; Diebold et al., 2013).

Inside the microscale computational domain it is necessary to characterize surface properties in terms of roughness lengths and forest canopies. Canopy models account for drag and added turbulence generation and dissipation in the wind profile. Again, RANS approaches are commonplace in forest canopy modelling not only for their consistency with ABL models but also for the need of fewer parameterization coefficients than higher-order closure models (Sogachev and Panferov, 2006). Parameterizing the canopy structure is the main challenge in the presence of heterogeneous forests. Aerial LiDAR scans have proved effective to provide a detailed mapping of the local forest height, drag coefficient and frontal area density (Boudreault et al., 2015).

3. Mesoscale to Microscale Downscaling

In general, we talk about downscaling when we relate large-scale and site-scale data to produce high-resolution time-series or distributions of variables of interest in connection to climate, high-resolution modelling or forecasting studies. This can be done using statistical or physical downscaling methods.

Statistical downscaling relates large-scale fields from meteorological models with local variables, typically measurements. The main objective of these methods is to reconstruct long-term high-resolution time series of target variables out of a short-duration measurement campaign and a long-term model integration. The main

advantages of these methods, compared to physical downscaling, are their low computational cost and high representativeness of local conditions through the use of local measurements. There are three large categories of statistical downscaling methods: weather classification, weather generators and regression methods (Wilby and Wigley, 1997).

In the NEWA context, statistical downscaling is typically related to the long-term extrapolation of the wind resource, measured at a site over a short-duration campaign. From a wind atlas perspective, statistical downscaling can also be used to improve the long-term representativeness of a high-resolution simulation of a few years to a multi-decade extent based on reanalysis or low-resolution mesoscale simulations.

In connection to high-resolution wind mapping and wind farm design tools, downscaling is related to the coupling of mesoscale and microscale models. Physical downscaling is used to resolve atmospheric scales at progressively higher resolution as we approach the area of interest. This is done by mesoscale models, which downscale from coarse global circulation model outputs (like reanalysis) to a few kilometers, typically using telescopic nested domains of increasing resolution. The unresolved part is parameterized using semi-empirical functions or reduced-order models.

Further downscaling down to microscale can be done by statistical or dynamical coupling of mesoscale and microscale models. The main challenge in doing this coupling is to interface models that are developed separately, each one with own assumptions and numerical solver. In doing so, it is also necessary to make sure that we are not double-counting microscale effects.

3.1. Dynamic Coupling

Mesoscale-microscale dynamic coupling proceeds with the physical downscaling process down to the microscale level using different fidelity levels: algebraic (Howard and Clark, 2007), linearized (Gasset et al., 2012), RANS (Castro et al., 2015) or a LES (Mirocha et al., 2014) model of the ABL. The first two introduce fast corrections so that downscaling can be used operationally in numerical weather prediction.

Internal coupling makes use of the same computational solver to transition from mesoscale to microscale keeping consistency in numerics and physical models and switching off the physical parameterizations that are now resolved, for example using the WRF model with LES boundary-layer scheme (Mirocha et al., 2014).

External coupling links two different solvers through a coupler that transforms mesoscale outputs into appropriate initial and boundary conditions for an offline microscale simulation.

One example is the PALM model (described in section I.5) which is specifically designed for atmospheric and oceanic flows. This LES-based model can be used in dynamic downscaling modes through large-scaling forcing and nudging procedures. Despite that this model will not be part of the NEWA model chain; these coupling methods will be further tested within the project and probably modified by the ForWind group with the purpose of using PALM for verification and validation purposes of other microscale models to support the model-chain development. The dynamic coupling with PALM will also help for the planning of the experiments in Perdigao and Kassel as well as for the

investigation of further idealized test cases like the transition of the flow from land to sea (validation with data from the RUNE experiment).

3.2. Statistical Coupling

Physical-statistical coupling avoids costly integrations of dynamic coupled models by introducing a statistical coupler, or transfer function, that links mesoscale wind climate statistics with microscale corrections for subgrid microscale processes.

Most physical-statistical methods are based on wind climate classification mechanisms, similar to those employed in statistical downscaling. Essentially, the wind climate is reduced to a few classes, each one associated to a high-resolution model of the local effects.

As mentioned above, the dynamical coupling will be employed during the course of the NEWA project in order to contribute to the estimation of uncertainties associated to different fidelity models and methods in the model-chain; however, since the high-resolution Atlas generated by the meso-micro model-chain should cover the whole European domain, statistical coupling approaches comes as more suitable cost-effective methods for the development of the operational model-chain system.

Several classification techniques are planned to be explored for the generation of the wind climate classes that will provide the input conditions to the microscale models. These techniques will be developed in connection with the procedures to transfer the information from the mesoscales to the microscale models in a physically consistent manner.

The range of methods explored will start with adapted versions of well-established techniques for low-order microscale models, namely the wind generalization technique (Badger et al. 2014; Troen et al. 2015); to continue with more complex classification approaches such as those based on Neural Networks (e.g. Barbouchi et al. 2015; Chavez-Arroyo et al. 2014). These groups will then be used to generate the momentum/energy quantities to provide either the boundary & initial conditions or be included as source terms in the momentum and energy equations of the microscale models (e.g. nudging methods of Jothiprakasam 2014).

4. Towards a Mesoscale to Microscale Model-Chain for Wind Energy

The ambition in NEWA is to develop a model-chain that can link mesoscale and microscale wind climate conditions consistently. The mesoscale part of the model-chain is focused on the development of a unified WRF model set-up for wind energy (see deliverable D3.1). This open-source code is the most popular mesoscale model for research and operational numerical weather prediction so its adoption in the NEWA model chain is relatively straightforward.

In contrast, at the microscale level there is a large variety of codes, with different fidelity levels and licensing options. Annex I provides an inventory of the models that will be used in the NEWA project. Here, the adoption of a unified code is not possible. Instead,

we shall speak about a unified downscaling methodology that can be adopted by the different codes to make them as consistent as possible with each other and with the mesoscale part upstream.

OpenFOAM is progressively becoming the preferred open-source CFD package to build atmospheric microscale models for wind energy applications. Several NEWA partners have different ABL solvers built on OpenFOAM using similar physical modelling based on RANS approaches. A unified OpenFOAM-based microscale model will be defined with the same philosophy of creating a unified WRF set-up for wind assessment. This open-source reference model-chain will be the baseline for benchmarking with other modelling approaches and for further model development and evaluation activities in NEWA.

As new changes are introduced, as a result of the model evaluation process, it will be possible to track these changes throughout the project with quantitative information about added performance on the reference model and how other models (more or less advanced) compare to this benchmark.

The initial stage to setting up a unified model is to verify that all the modelers speak the same language so that they would produce a consistent solution. Hence, regardless of the fidelity of the microscale models and before considering any meso-micro coupling, the degree of consistency in their solution needs to be verified.

The errors associated to any CFD simulation come from a large number of sources such as the conceptual/physics implementations, simulation setup and numerical design. From those sources, the numerical aspects, in particular the spatial terrain-surface discretization together with the adequate domain configuration are essential for the accuracy and numerical stability of the solution. Thus, in this project stage, it has been decided to verify those numerical and methodological aspects from each model, evaluated both individually and in common cases, to be able to get to a common procedure for the simulation of wind flow over terrain which minimizes the numerical errors.

To this end, grid sensitivity analysis around complex terrain sites has been conducted. This exercise will also help defining best practice guidelines for the setting up and quality-check of microscale grids, a fundamental step in minimizing user-dependencies.

Table 1: Overview of the partner involved in the different test cases and each associated model.

Partner	Model	Solver	Test Case		
			Kassel	Perdigao	Alaiz
BSC	Alya (Avila et al. 2014)	Alya		x	x
CENER	CFDWind (Sanz-Rodrigo et al. 2009)	OpenFOAM v2.4			x
DTU	WAsP-CFD (Bechman, 2013)	EllipSys3D		x	
Franhoufer	IWES (Chi-Yao, 2015)	OpenFOAM v2.1	x		
CENAERO	IWES (Chi-Yao, 2015)	OpenFOAM v2.1	x		

It is important to mind that this analysis aims at indicating the best practices towards the evaluation of the numerical requirement for microscale CFD models used for wind resource assessment. The study does not tell whether the model is well suited for predicting actual terrain flows.

Table 1 shows the list of models verified in this report, together with the partner that manages, support and/or uses each model. In addition it is shown the test case used by each model to perform the grid independence study.

5. Test Cases

NEWA plans three experiments of increasing terrain complexity: Kassel (Germany), Perdigão (Portugal) and Alaiz (Spain). These sites have been included in the initial sensitivity tests for the mesoscale and microscale modelling groups because in addition to the verification activities, the simulations will be used to support the design of the experiments.

The main characteristics of each site are described below. Each of them has certain parameter range that has not been covered by field experiments in the past. So they will provide extensive and valuable information for the deeper understanding of the wind flow over a wide variety of terrain complexities and climate conditions.

Therefore, they are the obvious starting point for the grid sensitivity study performed in this project stage. Choosing these sites will also serve for the steps in the development and validation of the model-chain methodology in the next project phase.

5.1 Kassel: Forested Hill

The experiment at Rödeser Berg locates in Wolfhagen around WWN 15km away from Kassel, Germany. This site is remarkable for the 200m Met. Mast (51°11'25'', 9°11'42''), which is currently the highest met. mast in Germany; also, the second one (140m height) is under construction located at (51°21'18'', 9°10'1.2'').

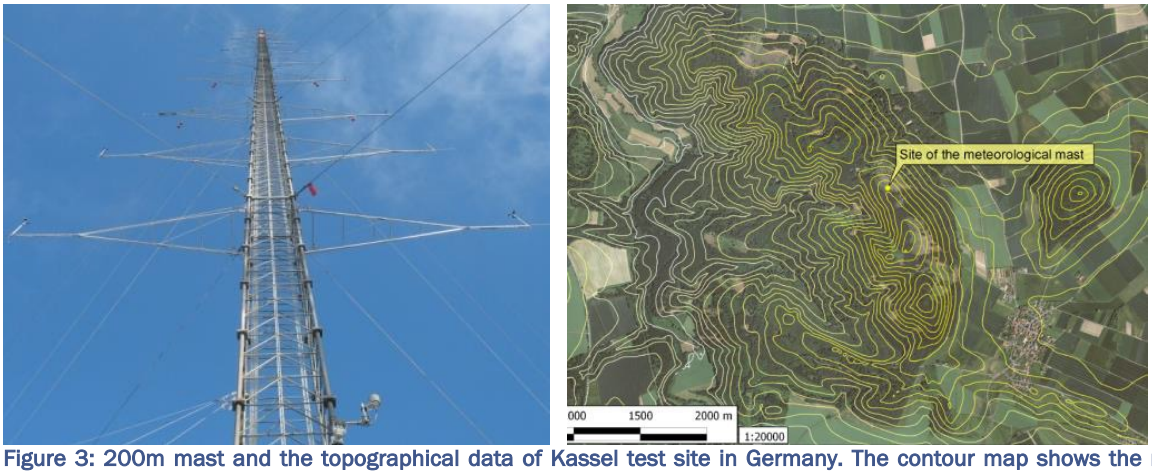

Figure 3: 200m mast and the topographical data of Kassel test site in Germany. The contour map shows the ridge direction of NW and the flat surrounding region.

From the orographic point of view, the ridge in the NS - SE direction has a peak altitude of 419m. The hill area is covered by the forest whereas the surrounding region is rather flat and can be described as farm land, where the altitude is around 219m. Besides, there are 4 turbines existing on the downwind side of the hill (Figure 3).

Since the prevailing wind direction is SSW, the wind passes the flat region, speeds up due to the topological characteristics and is blocked by the vegetation, then creates the recirculation zone in the down-wind side of the hill. Under this consideration, the second 140m Met. Mast, together with the LIDAR measurement could deliver the entire flow patterns over the forest hill, see Figure 4.

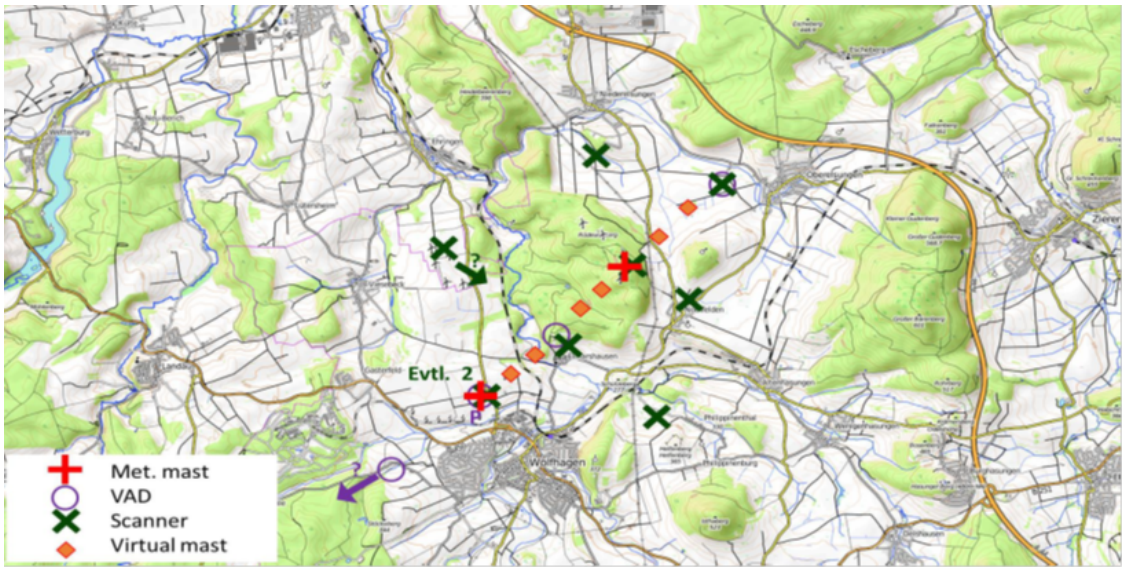

Figure 4: Location of the existing and constructing met. mast, the planed scanner and the virtual mast for the complete flow pattern around the hill

As concluded by the two comprehensive reviews of Finningan (2000) and Belcher et al. (2012), the interaction between complex terrain features and forest elements is still a challenge to the micrometeorologist and a forefront area of research.

Therefore, despite that both, the Perdigão and Alaiz sites are partially covered by forest canopy; the Kassel site has a particularly very dense forest covering the entire hilly area of study. Because of the characteristic lengths involved in these elements, the Kassel experiment will be ideal for the deeper understanding of the wind flow over forested areas

5.2 Perdigão: Doble Hill

Referring to the reports of task 2.2 of NEWA (Palma et al. 2015) as well as the report of Bechmann (2016), the Perdigão site, located in the centre of Portugal, contains two approximately 500 m high parallel ridges with a distance of about 1.2 km. The ridges are about 4 km long aligned with the 318°azimuth.

A 2 MW Enercon E-82 wind turbine (WT) with 82 m hub-height and a 200 m tall meteorological mast (MET) are located on the western ridge at position (607587.0; 4396060.0) and (608384.7; 4395088.0) respectively (UTM WGS 1984 Zone 29).

Figure 5 shows both positions together with the overview of Perdigão with vertical scale magnification of 3x.

The eastern ridge is characterized by an orographic depression. Apart from the two main topographic elements, Perdigão is surrounded by flat terrain which is covered by only few land use types.

Figure 5: Overview of the Perdigão site showing the WT and MET positions on the western ridge (picture from Google Earth with vertical scale magnification 3x, extracted from Palma et al. 2015)

As explained in Palma (2014), this site is of particular interest for the understating of complex terrain processes since its orographic and land use features are characterized by parameter range that haven't been approached by any field study in the past (Fernando, 2014).

The steepness and altitude of its main topographic elements (the two hills) cause important wind flow separation which challenges the current state of turbulence modelling techniques (Palma et al. 2015).

On the conceptual side, as mentioned above, the site is surrounded by flat terrain covered by only few land use types providing a well-defined impinging flow.

Finally, the main characteristic is the two parallel ridges with dominant winds perpendicular to them. This is one of the best formations that nature can offer to mimic a sequence of periodic hills. So this site provides invaluable information for numerical modellers who require periodic boundary conditions and/or are limited to two-dimensions (Fernando, 2014).

5.3 Alaiz: Hill and Mountain Range

The Alaiz mountain range is located in Navarre (Spain), around 15 km SSE from Pamplona. The prevailing wind directions are from the North and from the South. To the

North a large valley is found at around 700 m lower altitude limiting to the North with Sierra de Tajonar, a 300 m high steep ridge. To the South, complex terrain is found with the presence of some wind farms, the closest one situated 2 km behind the row of six wind turbine stands of the test site. Five reference met masts, 118 m tall, are located in front of the turbine positions at a distance of around 250 m.

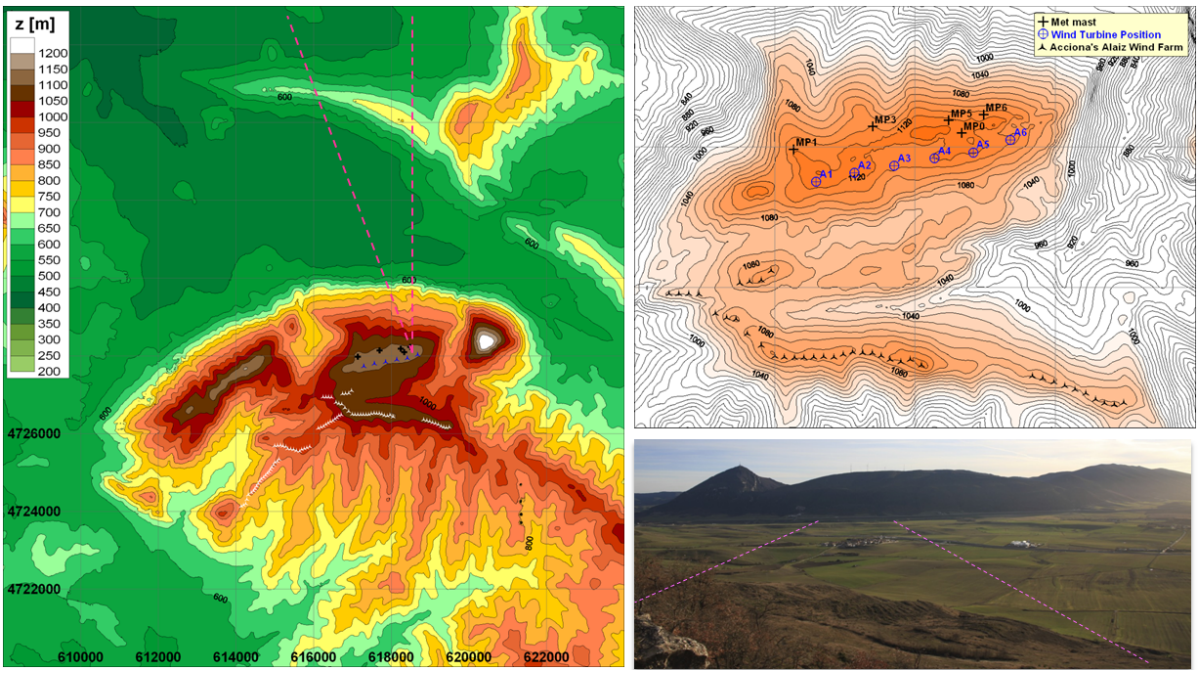

Figure 6: Orography of the Alaiz test site in Spain. Insert contour map with layout of CENER's test site and Acciona's Alaiz wind farm to the South. View of the Alaiz mountain range from the Tajonar hilltop to the North. The prevailing wind direction sector and foreseen instrument deployment area is marked with dash lines.

The site is characterized by two roughness levels. The western part of the test site, limiting with the MP3, position is covered with a dense canopy composed of bushes and beech trees 10-15 m high. The eastern part is covered by low bushes not higher than 0.5 m.

The test site has been operational since end of 2009 with the first wind turbines installed in the summer of 2011.

The flow field in Alaiz observed at the reference mast MP5 is highly dependent on the incoming atmospheric stability (Sanz Rodrigo et al., 2013). The mesoscale activity of the site has been characterized with consistently better results down to 0.5 km horizontal resolution using CORINE Land Cover land-use model (Correia et al., 2013).

At microscale level, several elements merit attention: 1) the interaction between the mountain and an upstream ridge to the North (Sierra de Tajonar); 2) the wake effects between CENER's test turbines and Acciona wind farm to the South; and 3) the interaction between terrain and forest canopy. The latter has been studied with CFDWind model using various canopy models (Chávez Arroyo et al., 2014). A summary of modelling results from different numerical models and wind tunnel measurements can be found in Sanz Rodrigo et al. (2014).

6. Complex Terrain Grid Sensitivity Study

6.1 Grid Sensitivity Approach

As stated in section 4, the main purpose of the grid sensitivity analysis carried out in this phase of the project is the verification of the numerical design of the microscale models that will be involved in the model-chain development. The results led us to an agreement in a best practice procedure that minimizes the numerical errors and reduces the user-dependency.

The purpose of the grid independency studies is to investigate how the accuracy of CFD solution depends on the resolution of the numerical grid. The grid independence analysis is in principle done by comparing the solution of a high-resolution grid to that of a lower resolution. As the results as directly associated with the underlying physics of each model, the first step in the collaborative grid sensitivity study was the agreement in a common conceptual approach (atmospheric surface layer concept described below). This partially allowed us to isolate as much as possible the sources of discrepancies among the various models to mainly their numerical design.

Still, the results of this analysis are also severely dependent on each CFD model because of their differences in discretization schemes, turbulence model, etc. However, because of the huge computational cost of testing all the possibilities, only few variables are selected by two participants provide a further insight to the model's sensitivity to numerical aspects in addition to the grid resolution.

Thus, while in the Kassel case the analysis is slightly focused in exploring the sensitivity of the IWES-OpenFOAM model (section 6.2) to some grid setup parameters, the grid independency study in the Perdigão site is complemented with a sensitivity analysis of the discretization scheme employed for the convective terms by the EllipSys3D model (section6.3). Finally, the grid independence analysis performed in the Alaiz site pursues the verification of numerical aspect between two codes: CFDWind and Alya (section 6.4) by using an identical grids and almost identical model setup and wind conditions in order to associate the discrepancies only to their numerical systems; this is, the discretization method, linear solver, etc.

In complex terrain large changes in wind speed can occur for small changes in wind direction. Sorensen et al. (2012) and Bechmann (2016) showed that, as expected, some wind directions will have larger numerical errors than others. Hence, in principle a robust grid convergent solution at a given site should include the analysis of all wind directions.

However, because of the huge computational cost involved in the simulation of 360 directions per grid level, different approaches were employed in the present report to address the directional variability. While Bechmann (2016) carried out 36 wind directions spaced equally every 10º for the Perdigão site The Alaiz test case was simulated with a particular focus on the very detailed north wind direction, for which the grid independence analysis was carried out with 10 wind directions spaced by 2º (i.e. from -10 to 10 º).

On the other hand, the Alya and IWES-OF model analysed single wind directions with the purpose of verifying the models (only comparison between models) and not in the full grid independence convergence for a given site.

A summary of the test cases employed by each model to perform the grid independence analysis is shown in Table 2 together with the wind directions, grid resolutions and other parameters considered by each model during the sensitivity study.

Table 2: Overview of the partner involved in the different test cases, their associated model and the variables tested for the grid sensitivity analysis.

Test Case	Model	Wind Direction	Grid resolution	Discretization scheme*	Domain characteristics	
					z_1+ [m]	Domain height++
Kassel	**IWES-OF**	**180**	**{10, 14, 19, 25}**	**SUDS/UDS****	**{1.058 , 1.19 , 1.54}**	**~{9, 18, 27}**
Perdigao	**Alya**	**46**	**{15, 30, 50}**	**SUDS**	**0.2**	**4**
	WAsP-CFD	**{0..10..350}**	**{10 ,20, 40 , 80}**	**{QUICK, SUDS, UDS}**	**0.05**	**~14**
Alaiz	**CFD-Wind**	**{0..2..10} , {180}, {350..2..358}**	**{15 , 30 , 60 , 120}**	**SUDS**	**0.5**	**10**
	Alya	**0**	**{15 , 30}**	**SUDS**	**0.5**	**10**

*SUDS: 2nd order upwind schemes, UDS: 1st order upwind schemes, QUICK: 3rd order scheme
** SUDS is used for discretization of momentum convective term while UDS for turbulent quantities.
+ z_1: 1st cell height
++ Domain height expressed as

Agreement on a common physical model.

As described stated in the NEWA report of Bechmann (2016), when calculating the wind resources following the European wind atlas concept, the CFD model is only accounting for the atmospheric micro-scales scales, i.e. the near-surface wind with horizontal scales typically ranging from a few kilometres down to a few meters. Coriolis effects tend to act on longer scales and can be neglected. The effect of stability is assumed to be small perturbations to the primary neutral state and is also omitted from the simulations performed for this study.

This approach is commonly termed as the atmospheric surface layer model, as it complies with the surface layer theory as showed by Richards and Hoxey 1993 for two-equation turbulence models. The simplifications are indeed very often used in the wind engineering community.

Despite its limitations, the assumption of neutral stability and the omission of Coriolis effects cause the simulated wind to be independent of the Reynolds number. Therefore, CFD results are only dependent on the inflow direction and on the inflow profiles that are specified as a function of a far-field surface based on simple equilibrium conditions (Richards & Hoxey, 1993).

This approach also simplifies the grid independency study since we can either compare speed-up ratios or wind speed values (Bechmann, 2016).

On the other hand, the four wind flow models participating in this phase are based on RANS-based Eddy-viscosity turbulence closure. They all employ the standard the $k-\epsilon$ turbulence model of Launder and Spalding (1974). However they employ different set of turbulence model constants (listed in Table 3) whose implications are discussed in this report.

Table 3: $k-\epsilon$ turbulence model constants used by each model together with the value that satisfies the equilibrium profiles in horizontally homogenous conditions (Richards and Hoxey, 1993)

Model	κ	C_μ	$C_{\epsilon 1}$	$C_{\epsilon 2}$	σ_k	σ_ϵ	σ_ϵ **
Alya	0.41	0.0333	1.176	1.92	1	1.2381	1.2381
CFD-Wind*	0.4	0.0256	1.13	1.9	0.74	1.298	1.2987
WAsP-CFD	0.4	0.052	1.38	1.92	1	1.3	1.299
IWES-OF	0.4	0.09	1.44	1.92	1	1.4	1.111
IWES-OF+	0.4	0.033	1.176	1.92	1	1.3	1.1838

*Based on the set applied by Dettering and Ettling (1985)
** σ_ϵ values that satisfies the equilibrium profiles (Richards & Hoxey, 1993)
+ second set of constants tested with the IWES-OF model by the CENAERO group

Procedure for the analysis and error metric

The main application of the microscale models employed in the NEWA model-chain system is the detailed and accurate wind resource estimation over a certain region. Thus their numerical reliability should be proved this region defined as the target area.

Ideally, grid points in this area should be the same in all the grids used for the sensitivity study in order to avoid additional sources of error such as interpolation errors. Nevertheless, some grid generation systems, do not allow building multiple grids of different resolutions to preserve coincident nodes. While only the procedure and simulation system developed for the EllipSys3D model allows this consideration, it is also possible for the other mesh generators to setup a grid that minimizes the distance of points among the grids of different resolutions in the target area by defining proper domain centre and node positioning functions. The list of grid generator systems and their associated model are listed in Table 4.

An alternative approach in the CFD simulations commonly used for analysing the grid independence is the usage of single point or points over a line of the variable of interest to compare the evolution of its solution with the different grid resolutions.

In the present report, we used both approaches in order to conclude about each and to come up with more insights towards the future methodology employed for the NEWA model-chain.

Therefore, even though the CFD-model calculates velocity perturbations (speed-up) and turnings at all grid points, only the results at either the defined target area, or the specific points/profiles are extracted and used for comparison.

Table 4: Mesh generator associated to each model.

Model	Grid Generator	Horizontal domain configuration	Terrain treatment for reference conditions
Alya	Windmesh (Gargallo-Peiró et al. 2015)	Cylindrical with structured refinement in the centre	Blending function
CFDWind	Windmesh (Gankarski & Chavez-Arroyo, 2014)	Rectangular rotated with structured refinement in the centre	Blending function
WAsP-CFD	HypGrid3D (Sørensen, 1998)	Polar zooming grid	Blending function
IWES-OF	terrainBlockMehser (Schmidt et al. 2012)	Cylindrical	Smoothing function

For each grid level the fractional speed-up are calculated as follows (Bechmann, 2016):

$$\Delta S = \frac{u}{u_0} \quad (1)$$

where u is the simulated wind speed and u_0 is the reference wind speed at the same height above ground of the inlet velocity used at the simulated wind direction. Finally, the speed error is defined as:

$$\varepsilon = \left(\Delta S - \Delta S_{Q1}\right)\frac{u}{u_0}100\% \quad (2)$$

where ΔS_{Q1} is the speedup of the simulation performed with the finest grid (grid level 1).

here ΔS_{Q1} is the speedup of the simulation performed with the finest grid (grid level 1).

6.2 Kassel: Forested Hill

The grid sensitivity study of Rödeser Berg is executed using the model developed by Fraunhofer IWES based on the open source CFD package OpenFOAM (IWES-OF), for which the mesh are generated by terrainBlockMesher (see grid level 1 for model's details).

The model is based on the standard k − ε turbulence closure using SIMPLE procedure to approach steady state results (see section 1.4 for more details). The model constants used for the grind independence analysis are listed in Table 3 for the IWES-OF model (4th row). A final sensitivity test of the consistency of the model to different set of constants (4th and 5th row of Table 3) was also performed by GENAERO using the same IWES-OF model.

The approach to measure the grid independence is based on the comparison of the vertical profiles of wind speed chosen at the two mast positions described in section 5.1.

Simulation setup

As listed in table 2, the model is configured with second order upwind differencing schemes for momentum convective term whereas first order upwind differencing scheme are used for the turbulent quantities. The convergence criteria are set for $1 * 10^{-5}$ for all the variables.

As mentioned above, the Kassel site is analysed for a single wind direction of 180° (south direction). In addition to the grid resolution, this site was used for exploring the model's sensitivity to other two grid setup parameters: the first cell height over surface domains height. Some of the details of the compared grids are listed in Table 5.

Table 5: Detailed description of each mesh regarding the grid sensitivity study of Kassel site

Legend	Cell numbers	Domain height [m]	Grid size [m]	First cell height [m]
BASE-TM (finest Mesh)	21,760,000	4000	(10 10)	1.20
BASE (Baseline Mesh)	10,152,000	4000	(14.67 14)	1.19
1stCell-height	8,883,000	4000	(14.67, 14)	1.54
1stCell-low	10,786,500	4000	(14.67, 14)	1.06
domainHeight-high	12,436,200	6000	(14.67, 14)	1.19
domainHeight-low	7,106,400	2000	(14.67, 14)	1.19
gridRes-high	6,888,000	4000	(19, 18)	1.19
gridRes-low	4,200,000	4000	(26, 25)	1.19

CFD grid

All the cases were configured in horizontal domain, which consisted in a polar mesh of 30km diameter (see Figure 7). The roughness length is considered constant for the whole domain with a value of 0.3m.

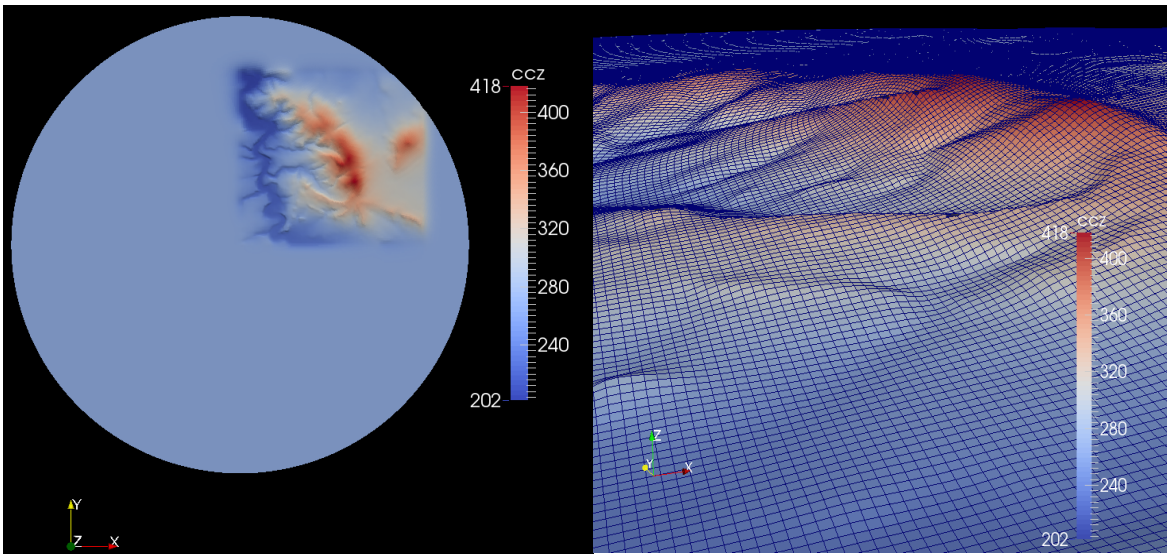

Figure 7: Domain of the Kassel site showing the elevation of the ground surface mesh (left). Closer view of the grid in the target area (right).

Boundary conditions

The inlet boundary condition was generated using the same equation system in one-dimensional column with periodic conditions at the sides. This methodology provides the

consistent solution for the three-dimensional domain and it is capable to avoid the numerical error provided by the inconsistency between equation system and analytical inlet profiles (see Chi-Yao, 2015). The conditions for the one-dimensional simulation are set such that the wind speed is 10m/s at 80m height on flat terrain.

In all the simulations, general wall functions are applied as the boundary conditions at the ground. These functions involve the destruction term (ε), turbulence production (G) and the turbulent shear stress according to the roughness similarity law

Simulation results

The results of the vertical profiles of velocity at the 140m and 200m mast locations are shown in Figure 8 and Figure 9 respectively.

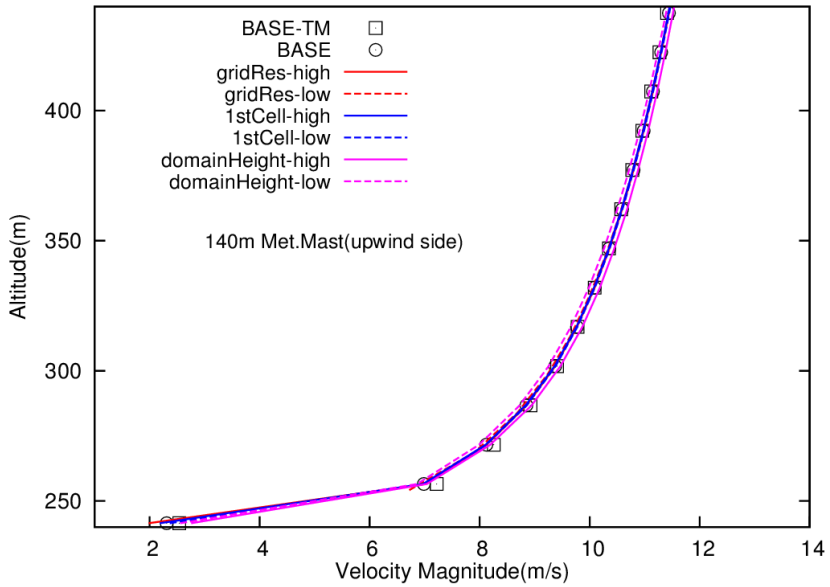

Figure 8: Velocity evolution of 140m met.mast location, upwind side of the forest hill.

The results show a very good agreement in the upwind side of the hill in which all the simulations have very similar representation on velocity.

The simulation results distinguish from one to another when the downwind side characteristics are concerned. Both, Figure 9 and **¡Error! No se encuentra el origen de la referencia.** show the under prediction of the velocity with the decreasing mesh resolution.

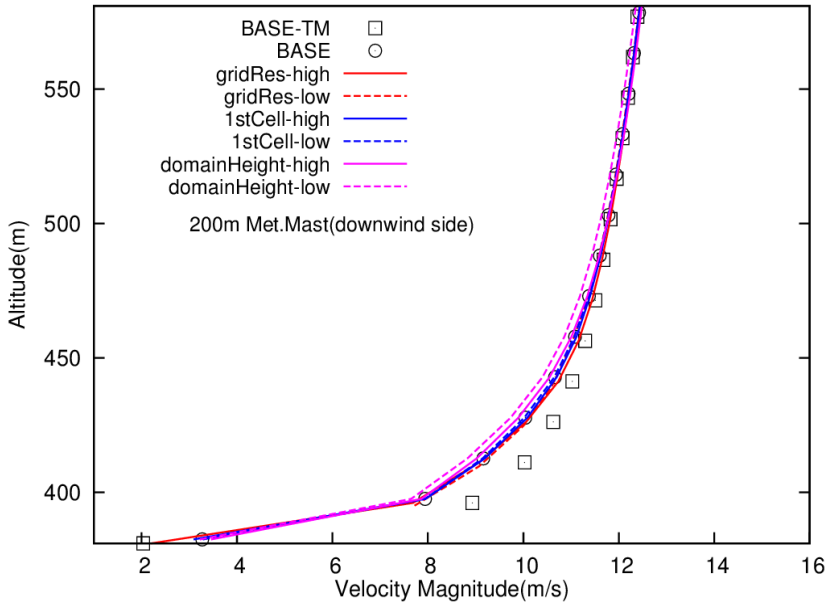

Figure 9: Velocity evolution of 200m met.mast location, downwind side of the forest hill.

Error analysis

The error plots are shown in Figure 10 and Figure 11 for the two mast positions. The errors are calculated as defined by eq. 2 considering the BASE-TM as the reference (finest) mesh. In can be well observed that the mesh induced numerical effect is much smaller in the upwind side, that is the 140m mast location (Figure 10), where the flow doesn't encounter a large manner of geometrical forcing. As the terrain complexity increases, i.e. towards the 200m mast (Figure 11), the demanded grid resolution becomes higher and the error in the near surface region becomes larger.

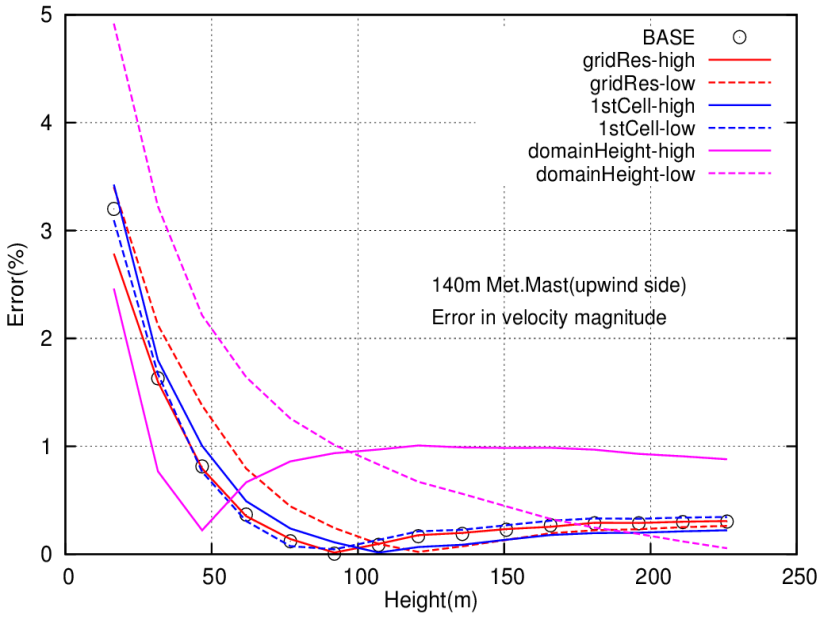

Figure 10: Evolution of the error in velocity at the 140m mast location (upwind side of the forest hill).

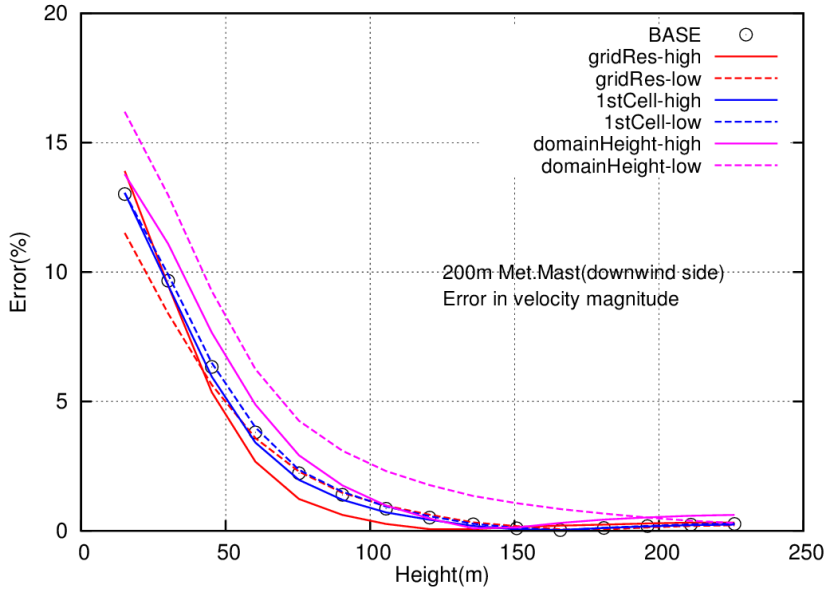

Figure 11: Evolution of the error in velocity at the 200m mast location (upwind side of the forest hill).

Nevertheless, the results in the hub height region (80-130m above ground) show very small deviation in all the tested mesh resolutions. This demonstrates a brief overview of the test meshes regarding their capability for the further numerical analysis.

Turbulence model consistency

An additional test was performed in the grid labelled as “gridRes-high” (see Table 5). This mesh was analysed with two model’s setups by using different set of constants of the turbulence model as listed in Table 3 (4th and 5th rows).

The results of the velocity vertical profiles with the two sets at the 200m mast position are shown in Figure 12 in which it can be noted important discrepancies between the wind profile, in particular from 40m up to 200m above ground.

According to authors such as Blocken et al. 2006 and Hargreaves & Wright (2007), the discrepancies might be produced by the unbalance of the constants in the standard $k-\varepsilon$ model whose constants have not been calibrated for atmospheric flows, with the equilibrium profiles of Monin-Obukhov as described by Richards & Hoxey, 1993.

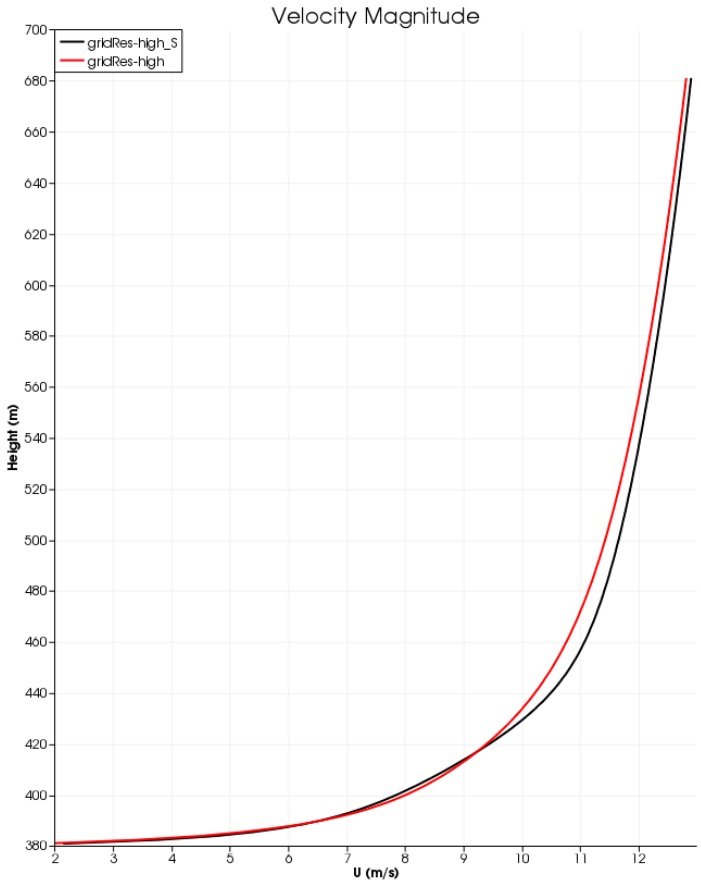

Figure 12: Comparison of the vertical profile of velocity obtained from simulations with the IWES-OF model using two different set of turbulence model constants.

6.3 Perdigão: Doble Hil

As listed in **¡Error! No se encuentra el origen de la referencia.** and Table 2, the grid independency study at Perdigao was carried out by two models: Ellipsys3D (section 1.I.2) and Alya (section 1.I.6). The analysis executed with Alya consisted only in comparing the sensitivity of the solution to the grid resolution (grid independence study) for a single wind direction. For this purpose, three grid resolutions were defined: 15m which is the finest grid (level 1), 30m (level 2) and 60m (level 3).

On the other hand, the analysis performed with the EllipSys3D code investigated no only the sensitivity of the results to the grid resolution for many wind directions, but also to the discretization schemes used for the convective terms. The grid independency study was based on the comparison of four grid resolutions (10, 20, 40 and 80m) at each 10º inflow direction, that is, 36 wind directions. The sensitivity to the discretization schemes was explored by comparing the third order QUICK scheme, which is operatically used by the model, with the second (SUDS) and first order upwind schemes (UDS) often used in the wind industry. This lead to a total of 432 cases simulated with the EllipSys3D model: 36 directions * 3 discretization schemes * 4 grid levels.

Terrain input information

The input data for both models were arranged by Bechmann (2016) by combining a 6x8 km area high-resolution terrain height vector map with SRTM data in order to make a 50x50 km orography map of Perdigão and its environs (Figure 13). Additionally, from the aerial laser scanning performed by Niras in April 2015, he was able to generate the ground roughness by using the method described by Boudreault (2015) in which the tree heights extracted from the laser scanning were converted to roughness values by assuming a roughness length equal to one tenth of the tree height.

Since the aerial scans only cover the two ridges a roughness length of 10 cm is assumed for the rest of the area, giving roughness values between 0.1 and 2.3 m.

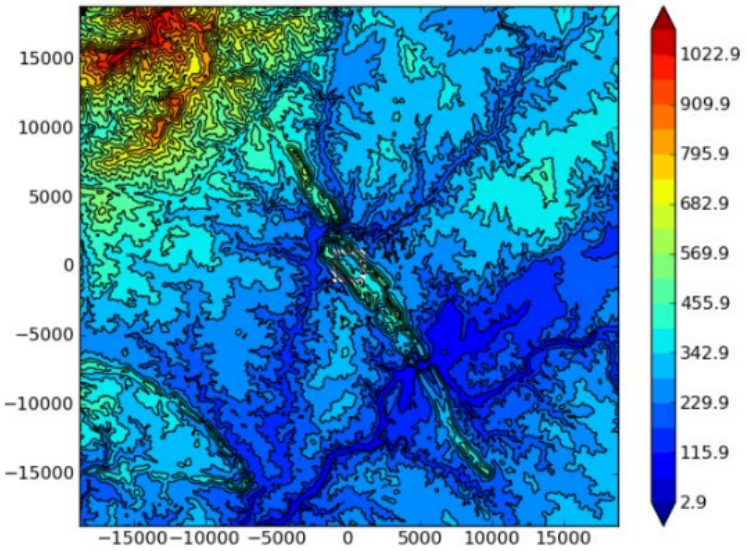

Figure 13: Orography map of Perdigao built by Bechmann (2016)

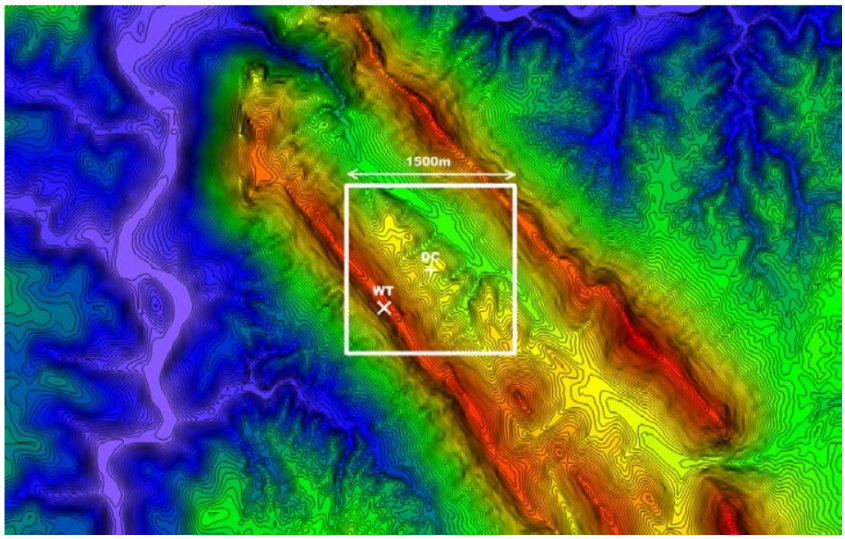

Figure 14: A close-up view the orography map used for CFD simulations (see section 5.2 for details). The figure shows the turbine position (WT) and the domain centre (DC) (Figure extracted from Bechmann, 2016)

The target area is a 1.5x1.5 km area centred at (608000.0; 4396400). It has been chosen so that both the WT position and the flow between the two ridges can be examined as illustrated in Figure 14. Even though the CFD-model calculates velocity perturbations (speed-up) and turnings at all grid points, only the results in this area are used both by the Alya and EllipSys3D model to define the reference conditions and to explore the effects of grid resolution by comparing each grid resolution level to the results of finest grid (level 1) as indicated by eq. 2.

6.3.1 EllipSys3D simulations

The complete study of the Perdiago test case with the EllipSys3D model is reported in Bechmann (2016). Below is presented the general procedure and overall results.

CFD model

Ellipsys3D code (the underlying code within WAsP-CFD) is a general-purpose flow solver used for many applications within wind energy. EllipSys3D is a multi-block finite-volume discretization of the incompressible Navier-Stokes equations in general curvilinear coordinates. More detailed description is provided in section 1.I.2.

On the advantages of EllipSys3D is the use of a multi-level grid sequence in steady-state computations to further accelerate computations. This multi-level grid sequence has the benefit of automatically making a grid independence test since EllipSys3D produces a result on each of the differently resolved grid levels. For grid independency tests one high-resolution grid is generated, and its solution (level 1) can be compared to the automatic solutions from a two times coarser grid (level 2), four times coarser grid (level 3) and eight times coarser grid (level 4).

For the present analysis, the code is used to solve the Reynolds Averaged Navier-Stokes (RANS) equations, and the numerical solution is only stopped when all variable residuals are below $1 * 10^{-5}$. Turbulence is modelled using the two-equation $k - \varepsilon$ of Launder and Spalding (1974), with fixed model constants calibrated for atmospheric flows as listed in Table 3 (3rd row).

Terrain treatment for reference conditions

Based on the terrain information, the EllipSys3D system requires to define the reference conditions for the model run.

The reference conditions in the direction in question are determined by the reference roughness, z_{0ref}, also called the “distant roughness” or mesoscale roughness. This is used when specifying the logarithmic inlet conditions and when calculating speed-up ratios according to eq. 1.

The reference terrain height, z_{ref} , is the “distance terrain height” in the direction of the sector in question. The model “flattens” the terrain toward this reference height and applies boundary conditions by the reference roughness. For each direction, the orography is flattened using the following blending function,

$$z_{CFD} = (1-\alpha)z + \alpha z_{ref} \quad (3)$$

$$zCFD=1-(\alpha z+\alpha zref \quad (3)$$

$$\alpha = \tanh\left(\left(\frac{d}{L_e}\right)^{\beta}\right) \quad (4)$$

$$= \tanh\left(\left(\frac{d}{L_e}\right)^{\beta}\right) \quad (4)$$

$$= \tanh\left(\left(\frac{d}{L_e}\right)^{\beta}\right) \quad (4)$$

$$\tanh\left(\left(\frac{d}{L_e}\right)^{\beta}\right) \quad (4)$$

$$(4)$$

where z_{CFD} is the resulting terrain height used for the CFD simulations, $\beta = 0.45$ and d is the distance from domain centre. For the present simulations, the reference terrain height for each direction is found at a distance of 13 km from the domain centre. The resulting orography after terrain flattening process is shown in Figure 15.

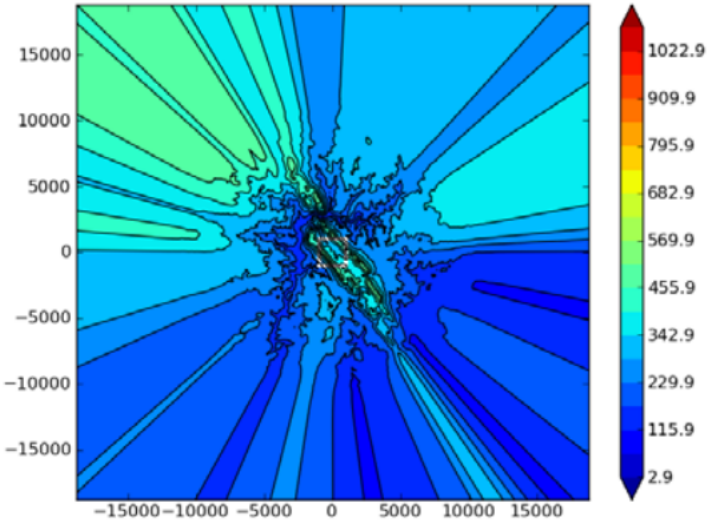

Figure 15: The figure shows how the far-field terrain for each direction is flattened toward the reference terrain height by the EllipSys3D model procedure of terrain treatment . (Figure extracted from Bechmann, 2016)

CFD grid and model's setup

Once the far-field terrain has been flattened the computational grid can be generated. Since ElliSys3D uses terrain-following coordinates, it is possible for the lower boundary of the computational grid to follow the orography. In this test case a high-resolution zooming polar grid is used. This polar structure allows to simulate any wind direction.

It consists of a central 3x3 km part with high grid resolution and an outer 30 km diameter polar part where the grid resolution gradually coarsens (see Figure 17). Instead of projecting the grid vertically when generating the surface grid, true surface projection is used to allow enough resolution even in areas of very steep terrain. The grid resolution of the reference finest grid in a direction following the terrain is 10 m in the central part.

An example of the lower boundary of the zooming grid is illustrated in Figure 16. As summarized in Table 2, to generate the 3D grid, the hyperbolic grid generator HypGrid3D Sørensen (1998) was used. Due to high-velocity gradients the near-wall, the grid cells are only 5 cm tall near the ground but gradually coarsens with height until the top of the domain is reached at about 9700m (Pedersen, 2010). This height is about 14 times the maximum difference in terrain elevation. The vast domain height has been selected to minimize the effect of blockage of the domain boundaries. 144 grid points are used in

the vertical direction and about 90 of these are employed in the first 300 m, giving a low vertical resolution of about 3.4 m in this region. Since the CFD-model uses a block-structured grid arrangement, the whole domain is divided into 180 3 blocks each of 48 cells or about 20 million cells in total.

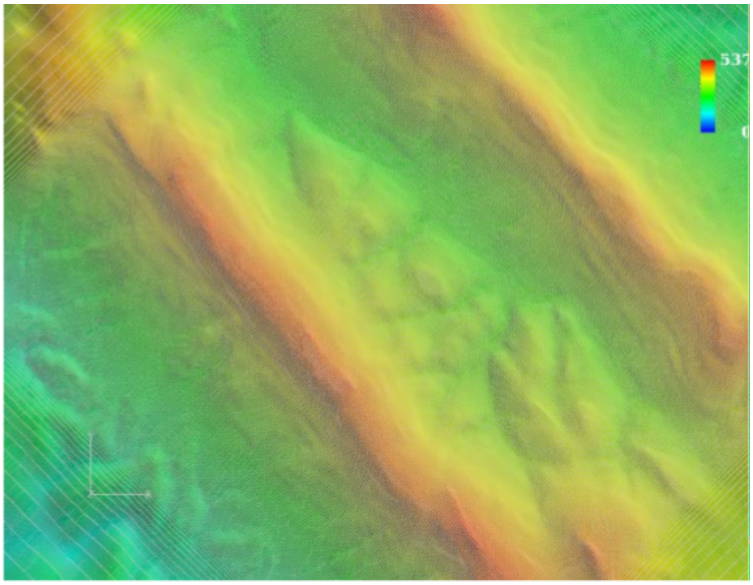

Figure 16: Closer view of the surface mesh created for the target area in Perdigao (Figure extracted from Bechmann, 2016)

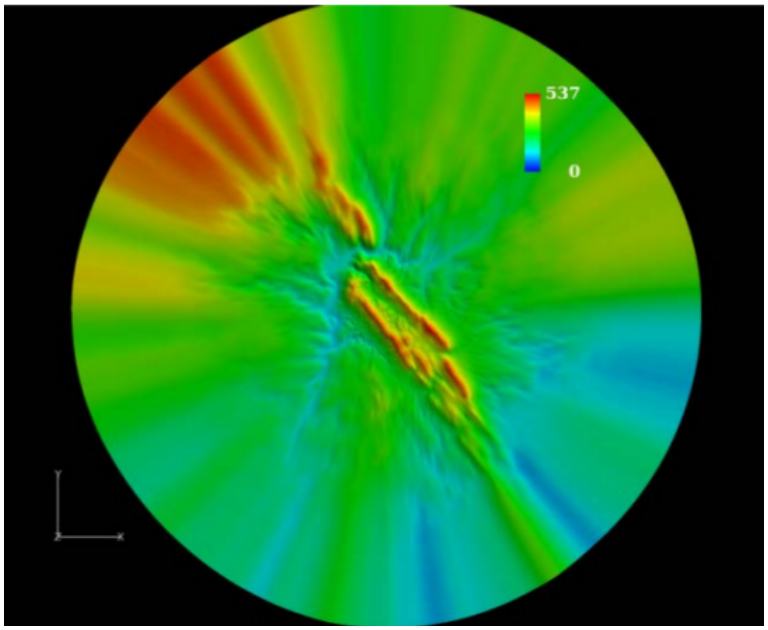

Figure 17: The 30 km diameter domain of the Perdigão site performed by the HyGrid generator (figure extracted from Bechmann, 2016)

Boundary conditions

The Logarithmic equilibrium profiles for the horizontal wind speed, u_0 , turbulent kinetic

energy, k, and the dissipation, ε, are used to specify the inflow conditions (Dirichlet conditions),

$$u_0 = \frac{u_f}{\kappa} \ln\left(\frac{z+z_0}{z_0}\right) \quad (5)$$

$$u0=u_f\kappa\ln z+z0z0 \quad (5)$$

$$k = \frac{u_f}{C_\mu^{1/4}} \quad (6)$$

$$\varepsilon = \frac{u_f^3 C_\mu^{3/8}}{C_\mu^{1/4} \kappa z} \quad (7)$$

$$= \frac{u_f^3 C_\mu^{3/8}}{\kappa z} \frac{u_f^2}{C_\mu^{1/4}} \quad (6)$$

$$= \frac{u_f^3 C_\mu^{3/8}}{\kappa z} \frac{u_f^2}{C_\mu^{1/4}} \quad (7)$$

$$uf2Cu1/4 \quad (6)$$

$$uf3Cu3/8rz \quad (7)$$

Outlet conditions are common Neuman boundary conditions. To be able to run different wind directions, each simulation specifies outlet conditions for 70 degrees of the downwind boundary while the rest of the horizontal boundary (290 degrees) is set as an inlet. Inlet conditions are also used at the top of the domain.

A wall function is used to model the effect of ground roughness. For EllipSys3D, the above described Logarithmic equilibrium profiles are used to derive the wall-function, see Sørensen (1995) and Sørensen et al. (2007b). As seen in eq. 3 the wall is placed on top of the roughness elements ($u = 0$ for $z = 0$) and is consequently displaced by the roughness length. This has been done to avoid a minimum height restriction of the first computational cell, and EllipSys3D can thereby resolve significant near-wall velocity gradients using shallow (high aspect ratio) computational cells.

Results

Figure 18 shows the mean absolute speed error in the target site for the 36 simulated directions at 5, 48 and 150m above ground for the different grid resolution and each discretization schemes.

In that figure is shown how that the numerical error increases for increasing resolution and for lower order discretization scheme. It is also seen that the error is larger close to the ground. As an example, the mean error at 150 m above ground for 20 m grid resolution is 1.4 %, 3.4 % and 7.1 % for the QUICK, SUDS and UDS scheme respectively. The numerical error is, therefore, more than 2 times higher when using a second order scheme and five times higher when using a first order scheme compared to the third order scheme. The same kind of increase in error is seen when the grid resolution is coarsened i.e. 1.4%, 3.3% and 6.1% error for 20 m, 40 m and 80 m respectively.

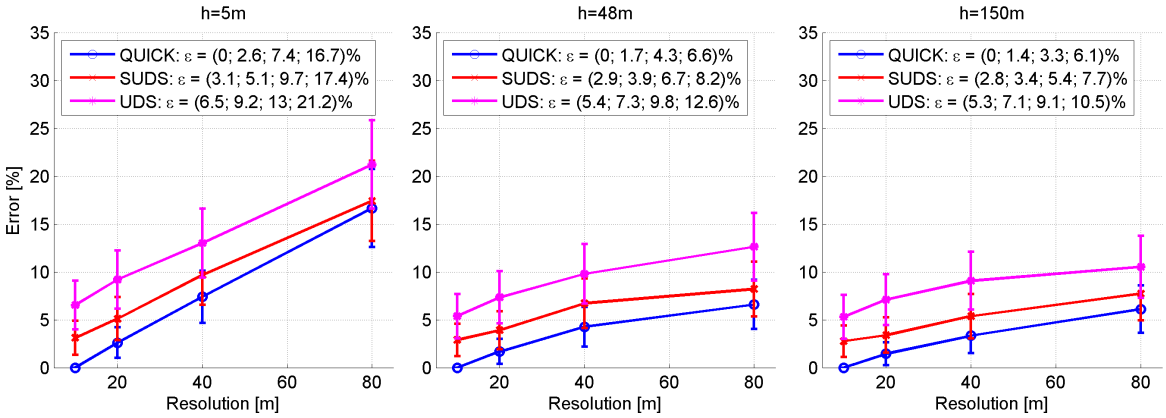

Figure 18: Mean absolute speed error as a function of grid resolution in the target site for 5 m (left), 48 m (middle) and 150 m (right) above ground. The results are the mean of 36 CFD simulations using the QUICK (blue), SUDS (red) and UDS (pink) discretization schemes.

Figure 19 shows the average absolute speed error at the WT-site. The results are an average of 36 simulations extracted at 48, 65, 80, 100, 120, 150m above ground. For 20m grid resolution the mean absolute speed error is found to be 0.8%, 2.1% and 4.2% for the three discretization schemes. The average error is, therefore, smaller at the WT-site compared to the average for the whole target site but still not negligible. In broad strokes the tendency that the error is doubled each time that the order of the discretization is schemes lowered or the resolution is doubled is repeated at the WT-site.

Sector averaged results for the WT-site can be found in the appendix of the T3.3 NEWA report of Bechmann (2016).

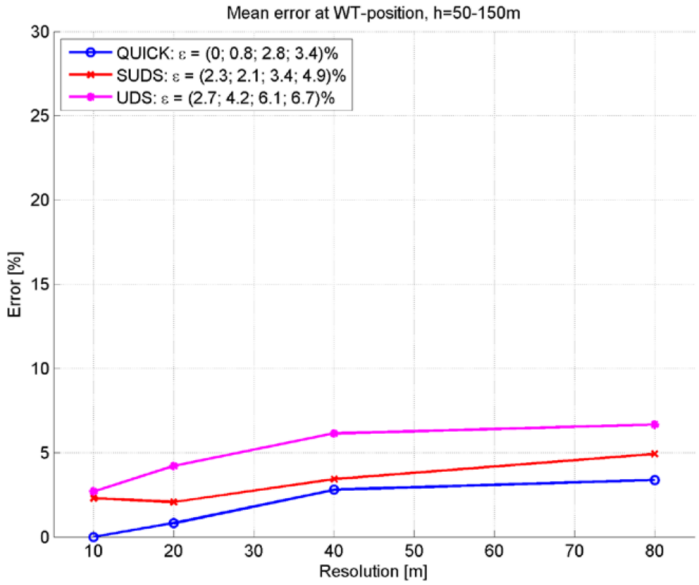

Figure 19: Mean absolute speed error as a function of grid resolution at the WT-position. The results are the mean of 36 CFD simulations, extracted at 48, 65, 80, 100, 120, 150m above ground using the QUICK (blue), SUDS (red) and UDS (pink) discretization schemes respectively.

6.3.2 Alya simulations

As mentioned above, the grid independence study at Perdiago is also carried out with the Alya model. The study is based on the error comparison of three grid resolutions. The reference mesh has a horizontal resolution of 15x15m (level 1),while the coarser meshes have a horizontal resolutions of 30x30m (level 2) and 50x50m (level 3) respectively.

Unlike the study carried out with EllipSys3D, only the 46° inflow direction was simulated in order to perform preliminary investigations towards the call for computations (Palma 2015) presented in the next stage of the project. This direction was chosen based on the call for computations. Nevertheless, the results from this direction are also compared whit the 30° sector results from the EllipSys3D model as they are based on the average of 3 wind directions. Despite the difference in inflow directions, this comparison can provide some insights of grid sensitivity differences between these two models.

CFD model

As described in section 1.I.2, the Alya code is a High Performance Computing multi-physics parallel solver based on finite elements and developed at Barcelona Supercomputing Centre. For this study, the model is used to solve the Reynolds Average Navier Stokes (RANS) by using the standard k-epsilon model for the turbulence closure. Linear elements are used for all variables, and an Algebraical Subgrid Scale Stabilization (ASGS) model is used to allow equal order interpolation for velocity and pressure and to deal with convection or reaction dominated flows.

CFD grid and model's setup

Alya model involves automatic meshing and generation of initial and boundary conditions for atmospheric boundary layer simulations. As summarized in Table 4, the automatic terrain mesh generator is called WindMesh-BSC. It generates block structured terrain-following meshes that maximize the quality of the mesh by applying mesh optimization techniques described in Gargallo et al. (2015). A view of the surface grid in the two ridges is shown in Figure 20). All grids are built on cylindrical-type domains with a diameter of 30 km, in which the grid size is finer in the central region as shown in Figure 21.

The finest, level1, mesh is defined a horizontal grid resolution of 15x15 m over a 7x7 km area centred in the central valley between the two ridges. Around this area the grid resolution gradually coarsens until reaching a horizontal mesh size of 300m at a diameter of 27km. The region outside the central 7x7 is used as a transition area where the terrain elevation is smoothly flattened until it reaches a constant height.

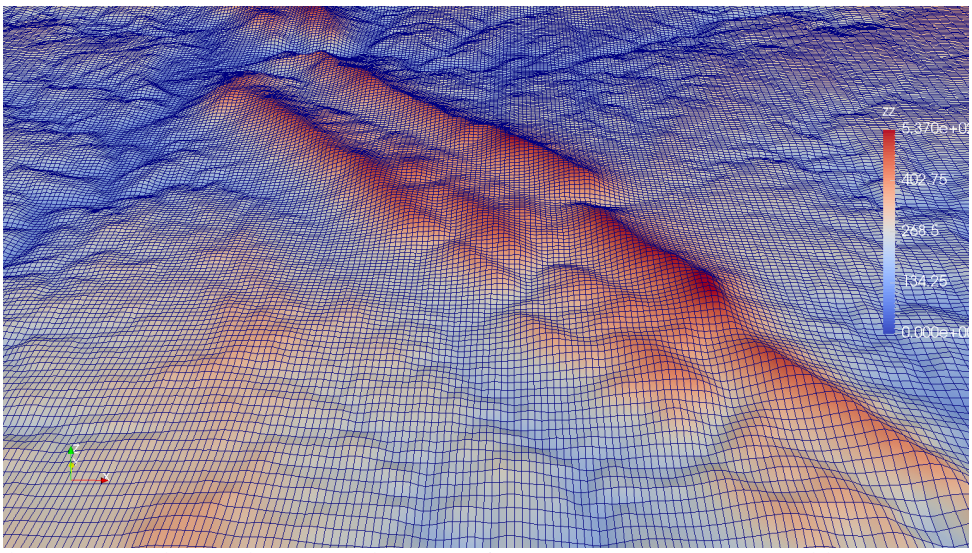

Figure 20: Close-up view of the surface mesh of the Perdigão site obtained by windMesh-BSC grid generation system.

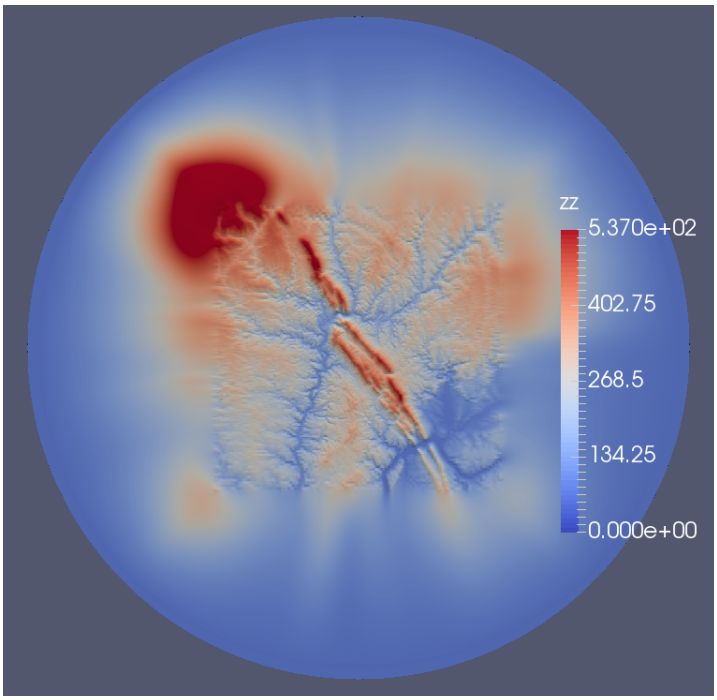

Figure 21: The 30 km diameter section of the Perdigão site is shown in the upper left side of the figure while the surface grid is illustrated in the right side.

The grid cells are 20cm tall near the ground but gradually coarsen with height until a maximum of 300m. The top of the domain is reached at about 2700 m. (4 times the maximum difference in terrain elevation). 48 grid points are used in vertical direction. The domain has 30 million of elements. The roughness was set to a constant value of 0.05 m over all the ground.

Boundary conditions

The imposed inflow boundary conditions for velocity, turbulent kinetic energy,k, and ε are solution of the atmospheric surface layer problem in homogeneous flat terrain (i.e. 1D problem) used as precursor simulation with the same roughness. This approach should lead to almost identical profiles of the profiles of eq. 3 – 5 employed by the EllipSys3D model.

Symmetry boundary conditions are imposed on the top boundary for the velocity, and turbulent quantities. The outflow boundary is set to zero normal gradient is imposed for velocity, k and ε. The pressure is set to zero.

The boundary conditions at the ground are based on a rough wall law. The height of the region modelled by the wall law is δw. In this region, two velocity scales u_{*v}, u_{*k}based on velocity u and turbulent kinetic energy k over the ground are defined as follows:

$$\boldsymbol{u_{*k} = k^{1/2} C_\mu^{1/4}} \tag{8}$$

$$\boldsymbol{u_{*v} = \frac{\kappa |u|}{\ln\left(1+\frac{\delta_w}{z_0}\right)}} \tag{9}$$

where $\kappa = 0.41$ is the Von Karman constant and z_0 is the wall roughness. The tangent

here $\kappa = 0.41$ is the Von Karman constant and z_0 is the wall roughness. The tangent

ere $\kappa = 0.41$ is the Von Karman constant and z_0 is the wall roughness. The tangent

re $\kappa = 0.41$ is the Von Karman constant and z_0 is the wall roughness. The tangent

e $\kappa = 0.41$ is the Von Karman constant and z_0 is the wall roughness. The tangent stress

$\kappa = 0.41$ is the Von Karman constant and z_0 is the wall roughness. The tangent stress

$= 0.41$ is the Von Karman constant and z_0 is the wall roughness. The tangent stress

$= 0.41$ is the Von Karman constant and z_0 is the wall roughness. The tangent stress τ_w

0.41 is the Von Karman constant and z_0 is the wall roughness. The tangent stress τ_w

$.41$ is the Von Karman constant and z_0 is the wall roughness. The tangent stress τ_w is

Von Karman constant and z_0 is the wall roughness. The tangent stress τ_w is

1 is the Von Karman constant and z_0 is the wall roughness. The tangent stress τ_w is

$=$ is the Von Karman constant and z_0 is the wall roughness. The tangent stress τ_w

$=$ is the Von Karman constant and z_0 is the wall roughness. The tangent stress τ_w is

s the Von Karman constant and z_0 is the wall roughness. The tangent stress τ_w is

the Von Karman constant and z_0 is the wall roughness. The tangent stress τ_w is

the Von Karman constant and z_0 is the wall roughness. The tangent stress τ_w is imposed

he Von Karman constant and z_0 is the wall roughness. The tangent stress τ_w is imposed

e Von Karman constant and z_0 is the wall roughness. The tangent stress τ_w is imposed

Von Karman constant and z_0 is the wall roughness. The tangent stress τ_w is imposed in

Von Karman constant and z_0 is the wall roughness. The tangent stress τ_w is imposed in

on Karman constant and z_0 is the wall roughness. The tangent stress τ_w is imposed in

n Karman constant and z_0 is the wall roughness. The tangent stress τ_w is imposed in

Karman constant and z_0 is the wall roughness. The tangent stress τ_w is imposed in

Karman constant and z_0 is the wall roughness. The tangent stress τ_w is imposed in

arman constant and z_0 is the wall roughness. The tangent stress τ_w is imposed in terms

rman constant and z_0 is the wall roughness. The tangent stress τ_w is imposed in terms

man constant and z_0 is the wall roughness. The tangent stress τ_w is imposed in terms of

$$\boldsymbol{\tau_w = -u_{*k} u_{*v} \frac{\boldsymbol{u}}{|u|} = -\frac{\kappa k^{1/2} C_\mu^{1/4}}{\ln\left(1+\frac{\delta_w}{z_0}\right)} \boldsymbol{u}} \tag{10}$$

which is linear for wall velocity $\boldsymbol{u}$. Zero normal gradient through the wall is imposed $\kappa = 0.41$ is the Von Karman constant and z_0 is the wall roughness. The tangent stress to kinetic energy k as a Neumann condition ($\nabla k \cdot \boldsymbol{n} = 0$). Finally, the imposed wall $\kappa = 0.41$ is the Von Karman constant and z_0 is the wall roughness. The tangent stress boundary condition for the dissipation ε is given by

$$\varepsilon = \frac{u_{*k}}{\kappa(\delta_w + z_0)} = \frac{k^{3/2} C_\mu^{3/4}}{\kappa(\delta_w + z_0)} \tag{11}$$

Simulated Cases

As already mentioned, the wind direction is set to 46° N, perpendicular to the ridges. The solution of velocity is extracted in the same target area as the one used with the EllipSys3D model (see Figure 14) and the fractional wind speed is computed using the same expression of eq.12. Thereafter, following the eq. 2, the error from the 30m and 30m grids are computed using the 15m grid resolution as the reference (level 1) fractional wind speed.

Results

Figure 22 shows the velocity errors over the target area. It is seen that the solution converges monotonically to the finer mesh. It is also seen that the error is larger close to the ground, however a very small difference is noted between the 5m and 48 m height results. Similar to the finding for all direction by the EllipSys3D model, the

numerical error is almost 2 times higher when the grid resolution is coarsened from 30 to 50m of grid size at the three heights.

When partially comparing with the results of the EllypSys3D model for a similar direction (sector) with the 3rd order QUICK discretization scheme as shown in Figure 23 it can be noticed a relatively smaller error in the EllisSys3D model when passing from the reference grid (10m) to the 20m grid, compared to the error in the Alya model when passing from the reference 15m grid to the 30m grid. That is from 2.8 to 6.8% at 5m from EllipSys3D and Alya respectively. This difference is however reduced to a difference from 2.4 to 3.8% at 150m. What is interesting to see from Alya model is the small difference between the 48m and 5m height results.

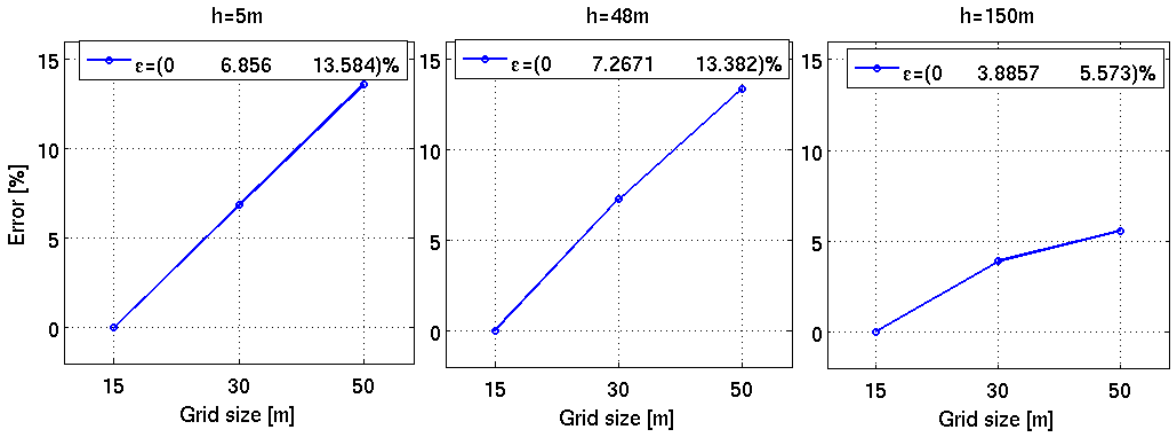

Figure 22: Mean absolute speed error as a function of grid resolution in the target site for 5 m (left), 48 m (middle) and 150 m (right) above ground for the 46° wind direction.

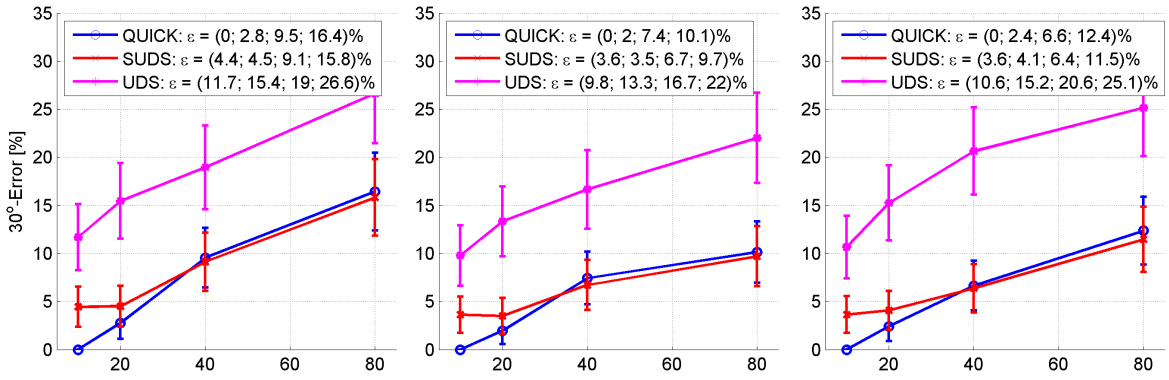

Figure 23: Mean absolute speed error as a function of grid resolution in the target site for 5 m (left), 48 m (middle) and 150 m (right) above ground. The results are the mean of 3 wind directions around the 30° sector using the QUICK (blue), SUDS (red) and UDS (pink) discretization schemes in the EllipSys3D model.

In addition to the differences in the numerical design between the models, and the wind simulated wind direction (46° vs. averaged 30° from Alya and EllipSys3D respectively) a potential sources of discrepancy is that during the convergence process of the Alya model, it was observed that the dissipation error did not converge monotonously with mesh size; this is due to the presence of spurious oscillations and the need to impose a

lower limit to this variable (clipping). Thus, further improvements are being made to the Alya code towards the model-chain development.

Comparison of EllipSys3D and Alya

Figure 24 illustrates the differences between the mesh generation systems used by EllipSys3D and Alya models. The HypGrid system (upper view) works on a polar system in which the flattening and blending function acts radially allowing a more efficient refinement in central areas. The windMesh system on the other hand allows a central refinement zone based on a squared area which can is more suitable to cover wider areas and, when aligned with the flow direction, minimizes the numerical diffusion. It is however; less efficient in terms of total number of elements as is passes from 20 to 30 million of elements despite it has half of the cell layers in the vertical direction.

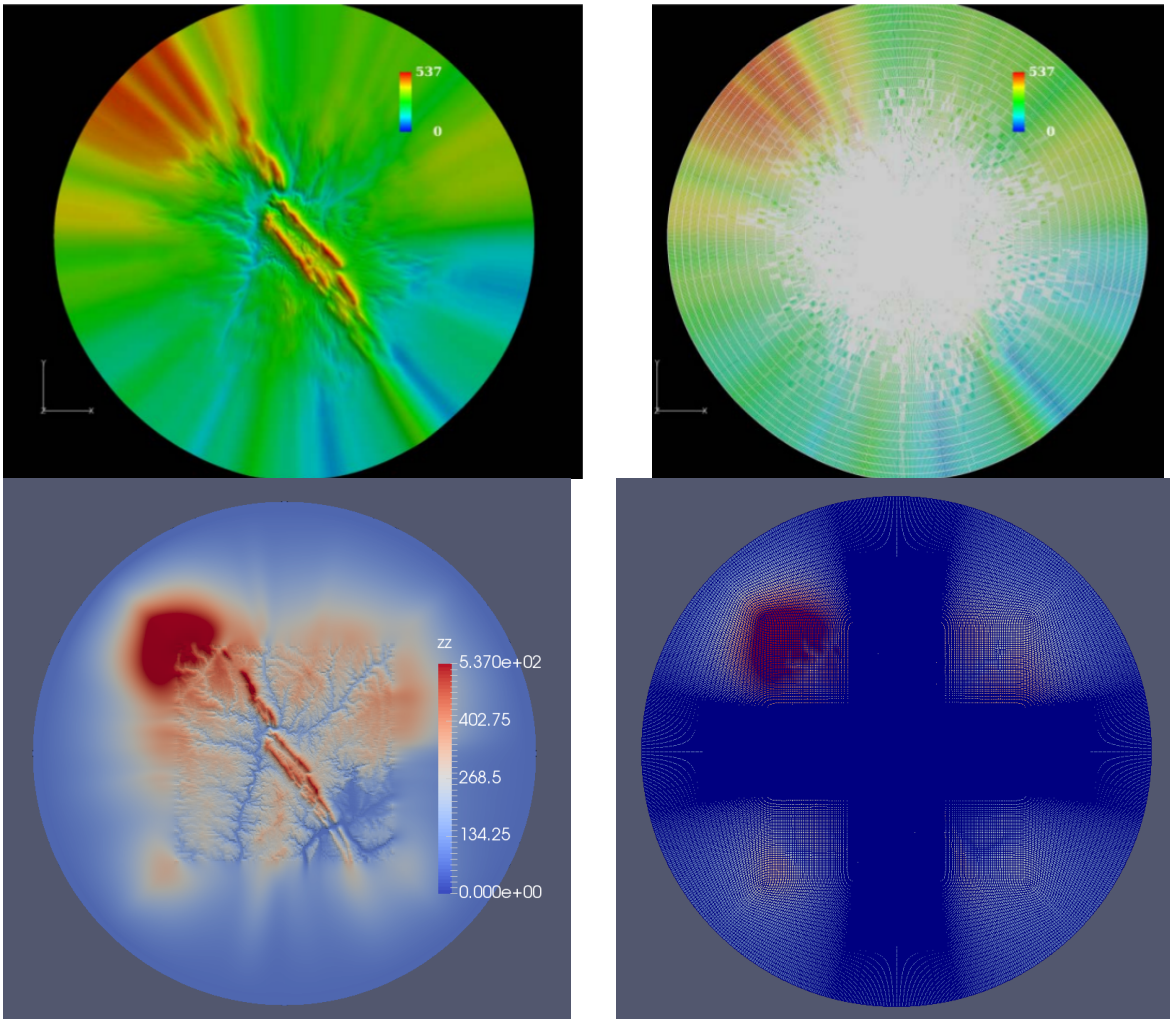

Figure 24: Illustration of the differences between the results of EllpSys3D (top) and Alya (bottom) grid generation systems. Left column shows the 30 km diameter section of the Perdigão site while right columns shows the surface grid approach used by each model

6.4 Alaiz: Complex Terrain

As listed in Table 2, the grid independency study in the Alaiz test case was carried out by two models: CFD-Wind (section I.1) and Alya (section 1.I.6).

Similar to the procedure followed in the previous test cases, the grid independence analysis carried out with the CFD-Wind model consisted in computing the evolution of the error among 3 grids, each with half of the cells' size than the previous mesh (30, 60 and 120m) when compared to the reference finest grid (level 1) built with a 15m resolution.

As has been mentioned before, the grid independency results depend dramatically on the wind direction since in complex terrain small changes in wind direction lead to large changes in wind speed (Sorensen et al. 2012; Bechmann 2016). However, because of the computational cost of running all grids in many wind directions, the grid independence analysis of CFDWind in Alaiz was performed for two wind direction sectors: north (0°) and south sector (180°) using the fact that in the Alaiz test case the real wind climate is characterized by a strong bi-directionality.

Despite the limitation in concluding a total grid-related error of the site with only two sectors, this approach provides complementary information to the procedure applied by the EllipSys3D code in Perdiago regarding the wind direction variability since the north direction was very detailed analysed by simulating the wind speed every 2° (from -10° to 10°) , that is 11 simulations. The southern direction was simulated only by the 180° direction in order to provide an insight of the Alaiz site sensitivity variability for tis two main wind sector.

As previously mentioned, the final analysis includes the comparison of the speed-ups and grid-convergence results between the CFD-Wind and Alya codes. To this end, both CFD-Wind and Alya were used to simulate the case of 0° wind direction in two identical grids. These grids correspond to the 15m and 30m grids studied for the grid independence analysis of CFDWind.

Terrain input information

The terrain information for both models is generated from digital elevation contour lines obtained from two data sources provided by the Navarra government, Spain (Navarra, 2015): 1): Topography maps of 1:5000 scale. Used for the Alaiz mountain (and up 3km far from the experimental test site) and 2) Topography maps of 1:10000 scale use for the rest of the surrounding domain. Both sets correspond to the year 2003 edition. After merging both data sets, the raster file is created through Delunay linear triangulation method in order to generate a regular grid with grid-spacing of 10x10 meters. The extent of the topographic data in shown

The target area in the Alaiz case was defined in Alaiz as a 3x3 km area centred in the point (618133.63 ; 4727980.1). This area has been chosen so that it covers the MP5 mast location together with the whole experimental Alaiz wind farm, as well as the main surrounding of the Alaiz Mountain affecting the wind farm. As in Perdigao test case, this area was used to extract the results of all the simulated directions to perform the grid independence study.

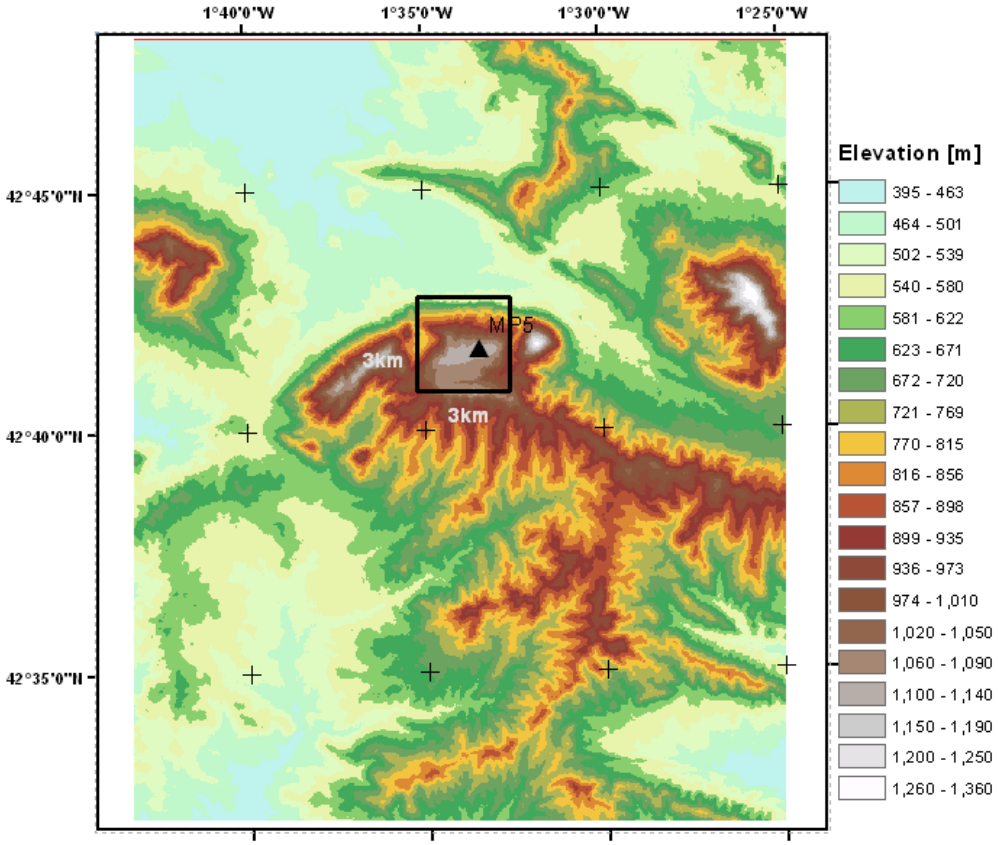

Figure 25: Orography map of Alaiz. The target area of 3x3 km is shown in the centre of the figure

CFD model and grid generator system.

CFDWind is a family of micro-scale models developed in CENER and build on top the OpenFOAM CFD software (OpenFOAM, 2015). This family is currently composed of three versions considering different physical complexity levels (see section I.1 for more details).

As stated in section **¡Error! No se encuentra el origen de la referencia.**, in this study it was agreed in applying the physical approach based on the atmospheric surface layer theory which complies with the Monin-Obukhov Similarity Theory (MOST) as proposed by Richards and Hoxey (1993). This modelling approach is implemented in the so-termed CFDWind version 1.0.

The model solves the incompressible RANS equations and turbulence closure is achieved by the eddy-viscosity theory and the standard $k-\varepsilon$ closure scheme with the constants calibrated for atmospheric flows as used by Dettering & Ettling (1985).

The coupling between pressure and velocity in the equations is solved by the well-known SIMPLE algorithm in case of the steady-state flows. CFDWind uses second order upwind schemes for the convective terms, and central differences for the rest of the terms in the RANS equations.

CFDWind employs an automatic terrain mesh generator called WindMesh-CENER (Gancarski & Chávez-Arroyo, 2014). This software was jointly developed by CENER and the BSC specifically to generate structured terrain-following meshes that maximize the quality of mesh parameters such as orthogonality and skewness by applying certain angle filters and elliptic smoothing techniques.

WindMesh can generate both, cylindrical and rectangular (Cartesian) types of grid domains. Despite that the cylindrical mesh can be used for any inflow wind direction, the rectangular domain can be aligned to the wind direction in order to minimize the numerical diffusion when low-order discretization schemes are used.

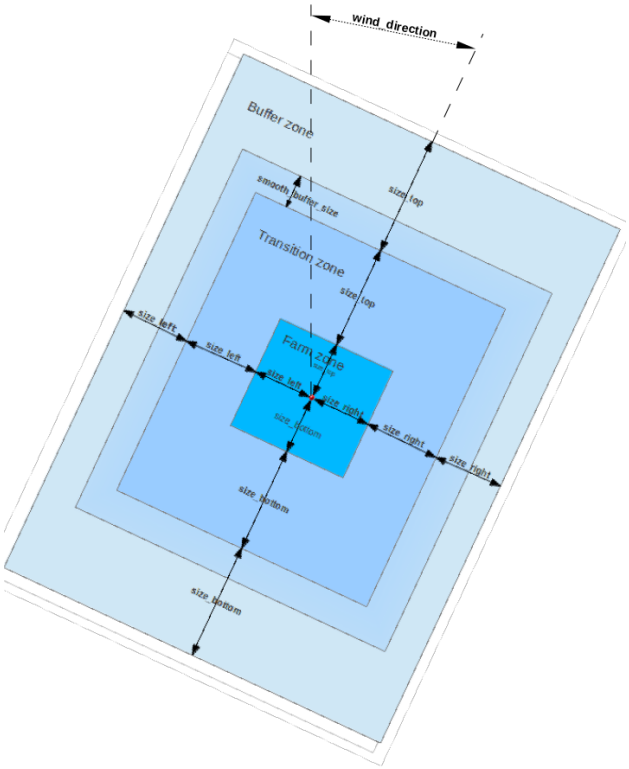

Figure 26: Illustration of the mesh structure defined by the mesh generator windMesh

Complex terrain should be avoided at the inlet and outer boundaries to be able to comply with the assumptions of inflow profiles, as well as to avoid any recirculation in the outflow. Therefore the terrain is smoothed far from the area of interest. To this end windMesh divide the terrain in different “zones” as illustrated in Figure 26. The central zone is called “farm” and in which the cells are refined to the maximum resolution established. Only real topography is considered for the grid generation in this region. Afterwards, in the called transition and smooth-buffer zone, the grid resolution is coarsened while the real terrain is blended with a function α (eq. 10-11) that is applied to the real topography data until it is flattened to a constant height in the a so-called buffer zone.

$$\alpha = \frac{1-\cos\left(\frac{d_{TZ}}{SB}\right)}{2} \qquad (12)$$

$$z = \alpha(z_B - z_T) + z_T \quad (13)$$

$$= \alpha(z_B - z_T) + z_T \quad (13)$$
$$= \alpha(z_B - z_T) + z_T \quad (13)$$
$$\alpha(z_B - z_T) + z_T \quad (13)$$
$$(z_B - z_T) + z_T \quad (13)$$
$$(z_B - z_T) + z_T \quad (13)$$
$$zB - zT + zT \quad (13)$$

where d_{TZ} is the distance to transition, SB is the size of the smooth-buffer zone and z_T is the terrain height in the SB zone.

CFD grid and model's setup

The base mesh (level 1) is a 15m resolution grid at the central "farm zone" whose dimensions are 7km x 10.5km wide and height, respectively. This area is built around the point (618133.63 , 4727980.0) with 7.5 km above the point, 3 km below and 3.5 km in the sides, always aligned with the wind direction as indicated in Figure 26. After this area of concentrated elements, the mesh resolution is coarsened to 150m 7km and 9km away from the centre in the wide and height directions until it reaches the flat terrain at 14.5 and 16.5km from the centre, leading a domain of 29x33km.

Despite this seems as complicated dimensions arrangements, the grid configuration is found to be more efficient when the target area is surrounded by very different terrain elements such as this case. That is, in the Alaiz test site, the simulations of the northern sector requires to account for the northern ridge of Tajonar because its high steepness creates a wake that strongly propagates because of the flat valley in from of Alaiz and affects the target site. However when the south direction is simulated, the Tajonar ridge is downstream the target area, so it doesn't need to be considered so it can be smoothed as part of the transition or buffer area. In the present study, the same previously mentioned domain sizing were used for the 11 north and the single direction south.

In a similar fashion to the windMesh version using by the BSC in the Perdiago test case, to build the 3-dimensional grid the surface grid (shown in Figure 27) is projected vertically following the normal vector of the terrain in order to maximise the orthogonality

Grid cells are 50 cm tall adjacent to the ground but gradually coarsens with height using a geometric function, until the top of the domain is reached at about 9km which is 10 times the maximum difference in terrain elevation. A total of 44 grid points in the vertical direction are used, leading to a mesh of about 30 million cells in total for the finest grid, around 8 million, 2 million and 0.7 million for the 30m, 60m and 120m resolution respectively.

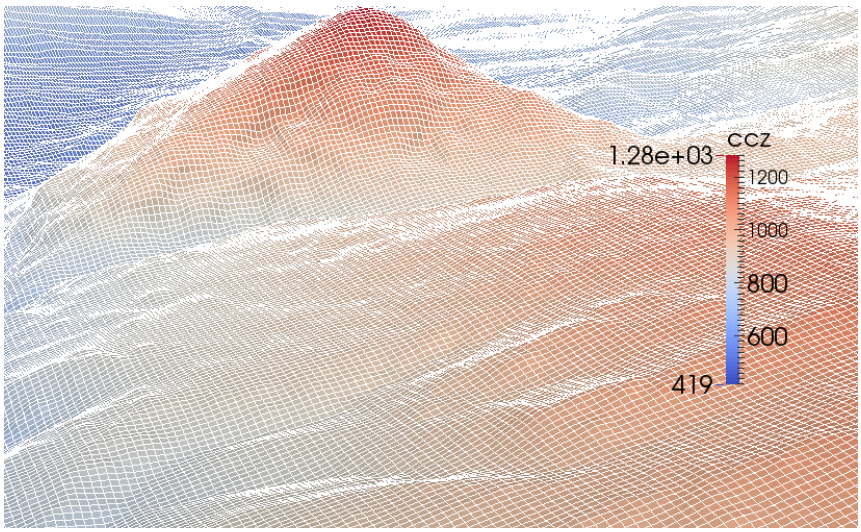

Figure 27: Close-up view of the surface mesh of the Perdigão site obtained by windMesh-BSC grid generation system.

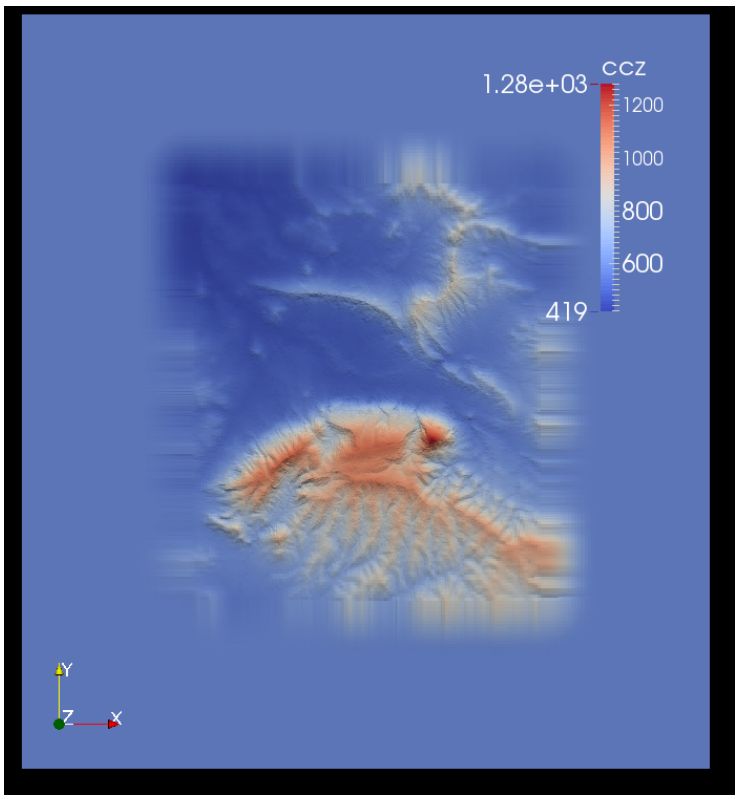

Figure 28: The 30 km diameter domain of the Perdigão site performed by the HyGrid generator (figure extracted from Bechmann, 2016)

Boundary conditions

The following (eq. 12-14) logarithmic equilibrium profiles for the horizontal wind speed, u_0 , turbulent kinetic energy, k, and the dissipation, ε, specify the inflow conditions based on the velocity scale at the inlet, u_*^0, calculated with a certain reference wind speed at a reference height, given the roughness, z_0, at the buffer zone. As the domain

is a rectangular, the conditions can be easily prescribed as Dirichlet conditions at the inlet face of the domain. Inlet conditions are also used at the top of the domain.

$$u_0 = \frac{u_*^0}{\kappa} \ln\left(\frac{z+z_0}{z_0}\right) \tag{14}$$

$$k = \frac{(u_*^0)^2}{C_\mu^{1/2}} \tag{15}$$

$$\varepsilon = \frac{(u_*^0)^3}{\kappa(z+z_0)} \tag{16}$$

Outlet conditions are common Neuman boundary conditions of gradient equal to zero.

At the ground, assuming wall bounded flow, the Richards & Hoxey (1993) wall treatment is implemented. Similar to Sorensen (1995), Parente et al. (2011) among others, the wall functions consider that the computational grid is placed on top of the roughness elements. So the restrictions related to the relation between the heights of the cells adjacent to the ground and z_0 are avoided. Consequently, the heights of the ground cells are considered as: $z_p = \delta_w + z_0$, where δ_w is the normal distance from each cell centre to their bottom faces.

Therefore, a horizontal kinematic shear stress (eq. 15) is applied to the momentum equation via an effective wall viscosity, ν_w. The shear stress at the wall is computed from local velocity scale, u_{*v}, in a similar fashion as defined by eq. 7 in the Alya model. To this end, the values of the velocity and turbulent kinetic energy (U_p and k_p respectively) of the cells next to the ground are employed to compute the local velocity scale.

$$\tau_w = \frac{\kappa C_\mu^{1/4} k_p^{1/2} U_p}{\ln(z_p/z_0)} \tag{17}$$

where the Von Karman κ and C_μ the constants from the $k-\varepsilon$ model. z_0 is the aerodynamic roughness length assigned to each cell in the ground.

The ε equation is ignored at the wall and its value prescribed according to the equilibrium expression for dissipation as follows:

$$\varepsilon_w = \frac{C_\mu^{3/4} k_p^{3/2}}{\kappa\, z_p} \tag{18}$$

Finally, as in Parente et al. (2011), by assuming local equilibrium, Neuman boundary condition for the turbulent kinetic energy is imposed whereas the value of its production rate term is replaced for the following term:

$$G_k = \frac{\tau_w^2}{\kappa C_\mu^{1/4} k_p^{1/2} z_p} \tag{19}$$

It should be noted that similar to the approach taken by Parente et al. (which differs from Richards & Hoxey (1993), Sorensen (1995) and Sumner & Masson (2012) , the production of k is not integrated over the first cell height since comparable to their

findings, a higher deviation in the second cell above surface was observed when MOST flows were simulated.

Results

Figure 29 shows the mean absolute speed error at 40 and 118m above ground in the target site for the two sectors simulated with the different grids resolutions. From the figure can be noticed that the error is drastically increased when passing from the 30m to the 60m resolution grid in which the error is doubled at both heights, passing from 2.8 to 5.6% and 1.86 to 3.9% at 40 and 118m height respectively.

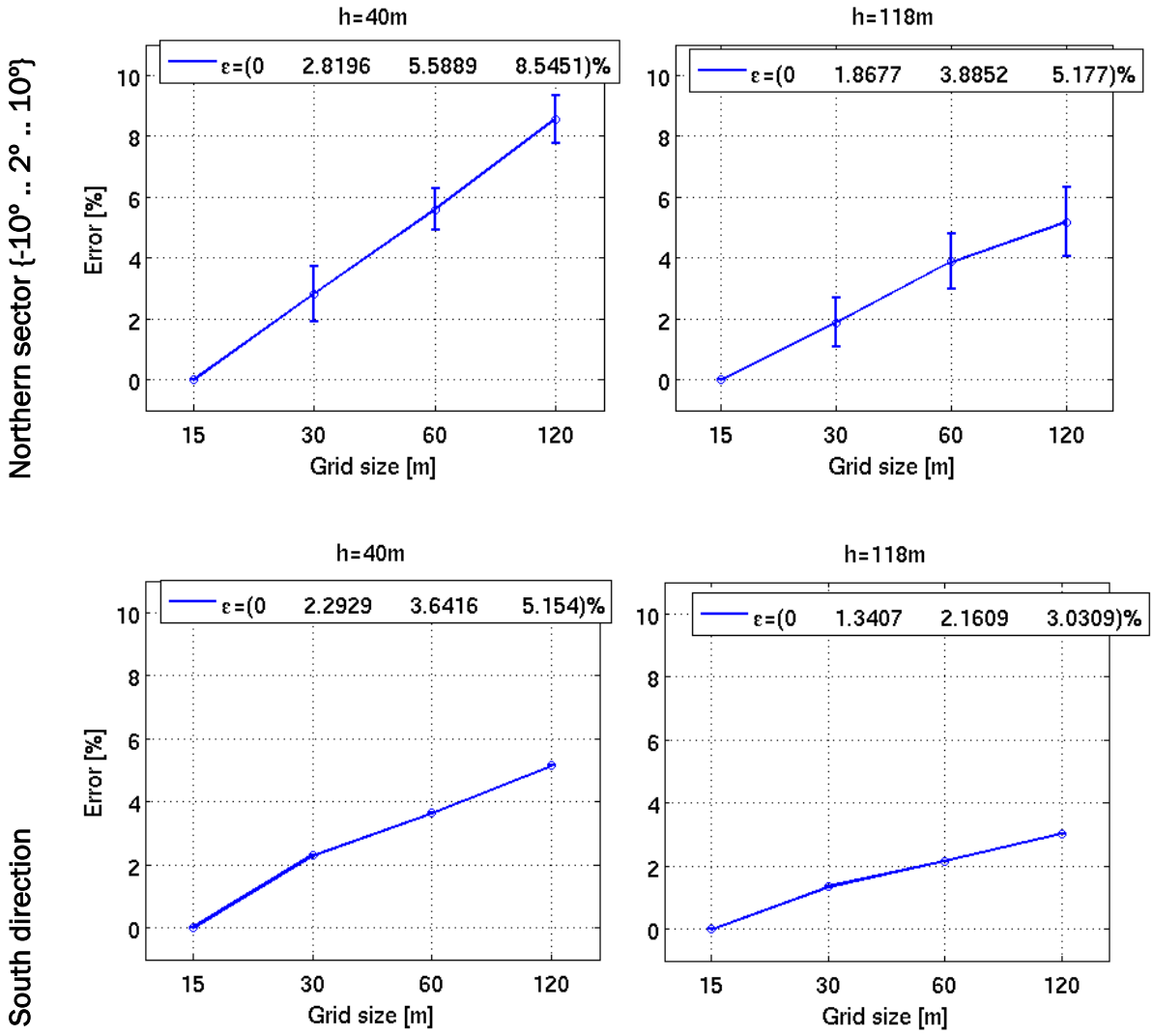

Figure 29: Mean absolute speed error as a function of grid resolution in the target site for 40 m (left) and 118 m (right) above ground. The results are the mean of 11 simulations for the northern sector (top) and for the single 180 wind direction for the south.

However, when passing from 60 to 120m the change is not as large; from 5.8% to 8.5% and from 3.8 to 5.1% for 40 and 118m respectively. On the other hand, very different results for the southern direction are found in which, despite simulating only the 180°

direction (unlike the averaged results for the north section) shows a smaller error as the mesh is coarsened with maximum values for the 120m resolution mesh of 8 and 5% at 40m and 118m respectively. These results agree with the part of the conclusion of Sorensen et al. (2012) and Bechmann (2016) regarding the large dependency of the wind independent results.

For the case of Alaiz, a possible reason is that the filters in the mesh generator have to process the terrain to assure that the model is numerically stable despite very coarse resolutions which contrast to finer resolutions in which the small size of the cells can accurately follow the terrain without losing quality such as the skewness, orthogonality, etc.

The spatial variability of the error for the north sector for each grid is shown in Figure 30. As expected, it is observed that the error is typically concentrated in the wake of the mountain in the lateral sides; downwind the MP5 mast and the Alaiz experimental wind farm (see Figure 25), where complex flow features such as recirculation and high vorticity in the flow is expected. As the resolution decreases, the differences with a finer mesh that captures more appropriately these features are increased.

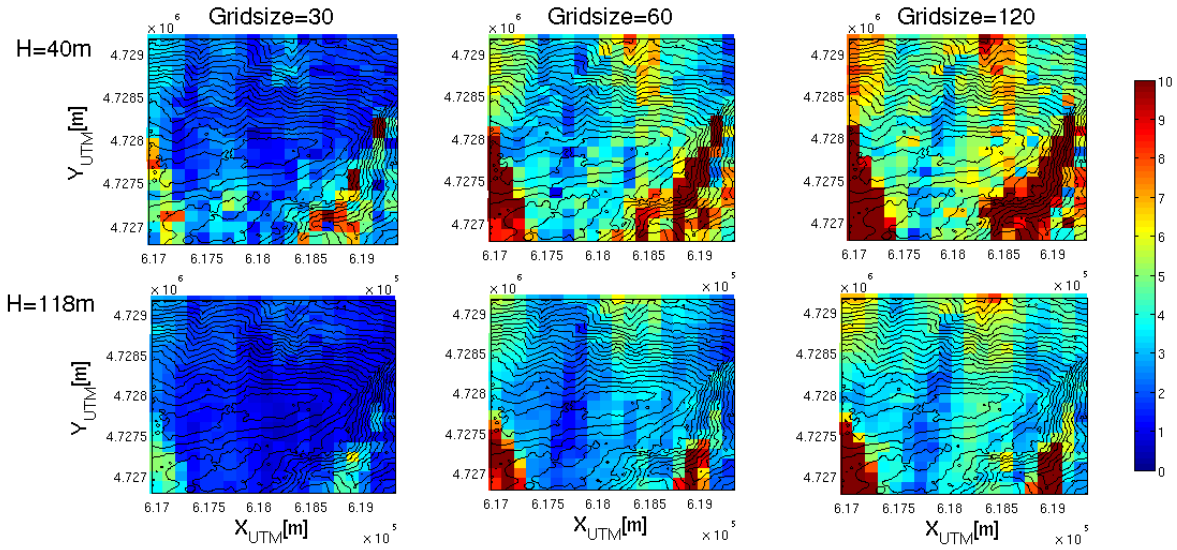

Figure 30: Spatial variation in the target area of the mean absolute speed error (among the 11 northern simulations) as a function of grid resolution for 40 m (top) and 118 m (bottom) above ground

Comparison between CFD-Wind and Alya

Finally, as summarised in Table 2, the CFDWind and the Alya model are used to simulate the 0° wind direction. The models setup is very similar and they use identical grids of 15m and 30m resolution employed in the previous independence analysis shown above for CFDWind. Figure 31 shows a histogram with the errors (eq. 2) at 40m above ground at every grid point in the target area, when comparing the 30m to the 15m resolution grid. It is seen a larger spread in the results of the CFDWind model compared to Alya, that is the grid independency can be higher in the Alya model.

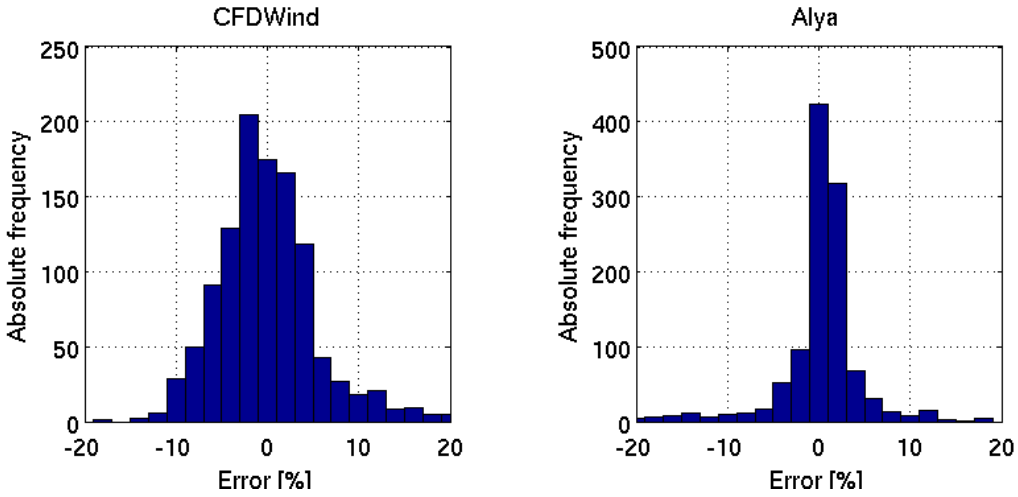

Figure 31: Wind speed errors at 40 m at every point in the target area for the CFDwind model (left) and the Alya model (right).

As the problem is independent to the Reynolds number, the comparison is made by computing the wind shear at all the points in the target area based on the ratio between the speed-up at 118m and the speed-up at 40m above ground.

As shown in Figure 32, despite the deviations seen between the models, which are most likely associated with the differences in their base numerical methods, a good agreement is found with absolute differences of 5.7% and 3.4% for the 15 and 30m resolution meshes respectively.

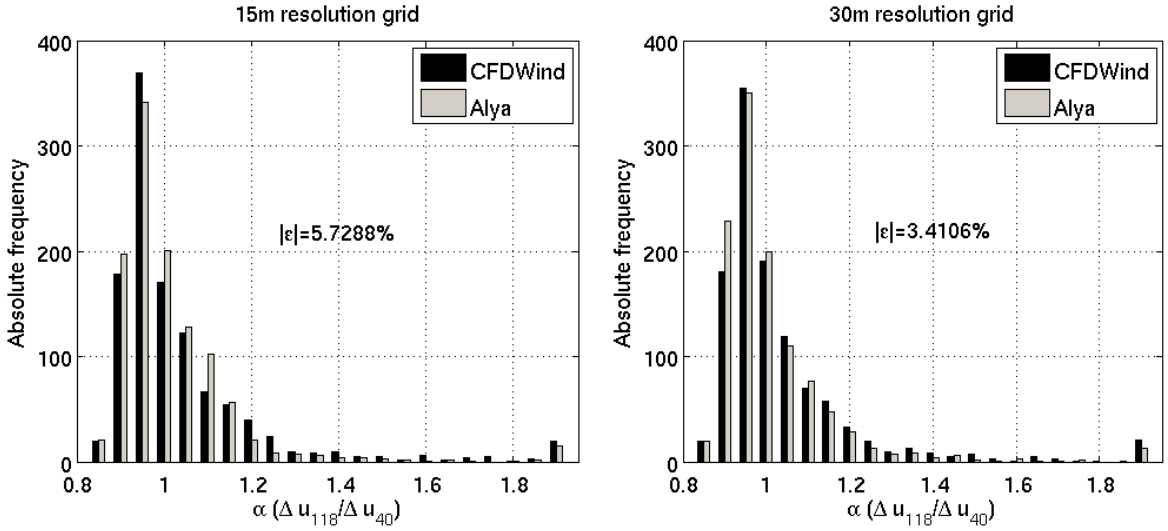

Figure 32: Wind shear in the target area computed as the ration of speed-ups between 118m and 40m for the 15m resolution mesh (left) and 30m resolution (right).

7. Conclusions and Outlook

This report presents the motivation for the development of a mesoscale to microscal model-chain for wind resource assessment applications. The initial efforts of the microscale modeling group in NEWA are directed to make sure the numerical errors are properly assessed before attempting validation against observational data. To this end a series of verification studies have been conducted with several CFD models with focus on grid dependencies in complex terrain.

Following the conclusions of the Perdigao study by Bechmann (2016), it has been seen how the CFD results will always have little numerical uncertainties despite the use of proper numerical techniques regardless of site and CFD model employed. This is aligned with previous work carried out by Sorenesen et al. (2012), where it was demonstrated that the convergence towards grid independency was slower than expected in the EllipSys3D code. Even with the very finest mesh they tested, with around a billion elements, the asymptotic range was not reached due to unresolved features in the terrain.

As grid independency in complex terrain is almost impossible to achieve in practical terms, it is important to have means to quantify the numerical error to make sure this is not significant enough to jeopardize any further model evaluation with observational data.

In practical terms, grid dependency will seek the right balance between computational cost and model resolution to ensure a manageable numerical uncertainty against other forms of uncertainties in the model chain (Bechmann 2016).

Running CFD models on coarse grids can cause significant erroneous results when assessing a wind farm power potential. This study can hopefully guide to choose a

proper microscale CFD setup and methods to assess grid dependencies to keep them under control.

Further work will be directed to incorporating more realistic characterization of surface properties affecting the surface-layer characteristics. In terms of physical modeling, the microscale group will incorporate atmospheric boundary layer physics to characterize the wind profile up to the free atmosphere. How to force this ABL with mesoscale input data will be another important topic in order to link with the wind atlas database.

References

Barbouchi, S., Dupont, E., D'All Ozzo, C., Giannakopoulou, M., Nibart, M., & Bonan, C. (2015). Modelling Methodologies To Estimate Annual Energy Production of Offshore Wind Farm. In Wind Resource Assessment Forum. London.

Beare RJ, Macvean MK, Holtslag AAM, Cuxart J, Esau I, Golaz J-C, Jimenez MA, Khairoutdinov M, Kosovic B, Lewellen D, et al. (2006) An Intercomparison of Large-Eddy Simulations of the Stable Boundary Layer. *Boundary-Layer Meteorol.*, 118: 247-272

Bechmann A, Sørensen NN (2010) Hybrid RANS/LES Applied to Complex Terrain. Wind Energy, 13: 36-50

Bechmann A, Sørensen NN, Berg J, Mann J, Réthoré P-E (2011) The Bolund Experiment, Part II: Blind Comparison of Microscale Flow Models. Boundary Layer Meteorol. 141: 245-271

Belcher, S.E., Harman, I.N. & Finnigan, J.J. (2012) The Wind in the Willows: Flows in Forest Canopies in Complex Terrain. Annual Review of Fluid Mechanics, 44(1), pp.479–504.

Berg J, Mann J, Bechmann A, Courtney MS, Jørgensen HE (2011) The Bolund Experiment, Part I: Flow over a steep, three-dimensional hill. Boundary-Layer Meteorol. 140: 1-25

Boudreault L-E, Bechmann A, Tarvainen L, Klemedtsson L, Shendryk I, Dellwik E (2015) A LiDAR Method of Canopy Structure for Wind Modeling of Heterogeneous Forests. Agric. For. Meteorol. 201: 86-97

Castro FA, Silva Santos C, Lopes da Costa JC (2015) One-way mesoscale–microscale coupling for the simulation of atmospheric flows over complex terrain. Wind Energ. 18: 1251–1272. doi: 10.1002/we.1758

Chávez Arroyo R, Sanz Rodrigo J, Gankarski P (2014a) Modeling of the atmospheric boundary layer in complex terrain with different forest parameterizations. Journal of Physics: Conference Series 524: 012119, doi:10.1088/1742-6596/524/1/012119

Chávez-Arroyo, R., Lozano-Galiana, S., Sanz-Rodrigo, J., & Probst, O. (2014b). Statistical-dynamical downscaling of wind fields using self-organizing maps. Applied Thermal Engineering, In Press.

Chi-Yao, C. (2015) Modification of inlet boundary conditions to improve the accuracy of CFD simulations for wind farm site assessment. Proceeding in Third Symposium on OpenFOAM in Wind Energy, Milan 2015.

Correia P, Lozano S, Chavez R, Loureiro Y, Cantero E, Benito P, Sanz Rodrigo J (2013) Wind Characterization at the Alaiz – Las Balsas Experimental Wind Farm using high-resolution simulations with mesoscale models. Development of a "low cost" methodology that addresses promoters needs. EWEA-13 proceedings, Vienna, February 2013

Diebold M, Higgins C, Fang J, Bechmann A, Parlange MB (2013) Flow over Hills: A Large-Eddy Simulation of the Bolund Case. Boundary-Layer Meteorol., 148: 177-194

Fernando, J. (2014). Microscale Modeling of Complex-Terrain Flows. Workshop at University of Notre Dame. Available at: http://www3.nd.edu/~dynamics/perdigao/microscalepresentations.html

Finnigan, J. (2000). Turbulence in plant canopies. Ann. Rev. Fluid Mech., pp.519–571

Gargallo-Peiró A., Avila M., Owen H., Prieto L., Folch A. (2015) Mesh Generation for Atmospheric Boundary Layer Simulation in Wind Farm Design and Management, Procedia Engineering 124, Pages 239-251.

Gibson MM, Launder BE (1978) Ground Effects on Pressure Fluctuations in the Atmospheric Boundary Layer. J. Fluid Mech., 86: 491-511

Hargreaves, D., & Wright, N. (2007). On the use of the k–ε model in commercial CFD software to model the neutral atmospheric boundary layer. Journal of Wind Engineering and Industrial Aerodynamics, 95(5), 355–369.

Holt T, Raman S (1988) A Review of Comparative Evaluation of Multilevel Boundary Layer Parameterizations for First-Order and Trubulent Kinetic Energy Closure Schemes. Reviews of Geophysics, 26: 761-780

Howard T, Clark P (2007) Correction and downscaling of NWP wind speed forecasts. Meteorol. Appl. 14: 105-116, doi: 10.1002/met.12

Koblitz T, Bechmann A, Berg J, Sogachev A, Sørensen N, Réthoré P-E (2014) Atmospheric stability and complex terrain: comparing measurements and CFD. *J. Phys. Conf. Ser.* 555: 012060, doi:10.1088/1742-6596/555/1/012060

Mirocha JD, Kosović B, Kirkil G (2014) Resolved turbulence characteristics in large-eddy simulations nested within mesoscale simulations using the Weather Research and Forecasting model, Mon. Wea. Rev. 142: 806–831, doi: 10.1175/MWR-D-13-00064.1

Navarra government (2015). Topographic information provided and licensed by the Navarra Government through the Ministry of Economic development (Orden Foral 1320/1998). Dataset publically available at: http://www.navarra.es/appsext/tiendacartografia/producto.aspx?id=2#13

Palma, J.M.L.M (2014) Perdigao. Field experimental planning and how US participants can help. Presented at: Microscale Modeling of Complex Terrain Flows, University of Notre Dame, Indiana.

Petersen EL, Troen I (2012) Wind conditions and resource assessment. WIREs Energy Environ, 1: 206–217 doi: 10.1002/wene.4

Richards PJ, Hoxey R (1993) Appropriate boundary conditions for computational wind engineering models using the k–ε turbulence model. *J. Wind Eng. Ind. Aerodyn.* 46-47: 145–153

Sanz Rodrigo J, Borbón Guillén F, Gómez Arranz P, Courtney MS, Wagner R, Dupont E. (2013) Multi-Site Testing and Evaluation of Remote Sensing Instruments for Wind Energy Applications. Renewable Energy 53: 200-210, doi:10.1016/j.renene.2012.11.020

Sanz Rodrigo J, Lozano Galiana S, Fernandes Correia PM, Cantero Nouqueret E, García Hevia B, Stathopoulos C, Borbón Guillén F, Chávez Arroyo R, Gankarski P, Koblitz T, Barranger N, Conan B (2014) Hierarchy of flow models and experimental support for wind resource assessment The WAUDIT-Alaiz complex terrain test case. EWEA-14 proceedings, Barcelona, Spain, March 2014

Sanz Rodrigo J, Chávez Arroyo R.A., Gancarski P, Moriarty P, Churchfield M, Clifton A, Kosovic B, Réthoré P-E, Hansen KS, Hahmann A, Mann J, Mirocha JD, Rife D (2016) Mesoscale to Microscale Wind Farm Modelling and Evaluation. WIREs Energy Environ, accepted for publication

Silva Lopes A, Palma JMLM, Castro FA (2007) Simulation of the Askervein Flow. Part 2: Large-Eddy Simulations. *Boundary-Layer Meteorol.* 125: 85-108

Schmidt, J., Peralta, C., & Stoevesandt, B. (2012). Automated generation of structured meshes for wind energy applications. In Open Source CFD International Conference. London.

Sogachev A Panferof O (2006) Modification of two-equation models to account for plant drag. *Boundary-Layer Meteorol*. 121: 229-266

Sogachev A, Kelly M, Leclerc MY (2012) Consistent Two-Equation Modelling for Atmospheric Research: Buoyancy and Vegetation Implementations. Boundary-Layer Meteorol., 145: 307-327

Sumner J, and Masson C (2012) The Apsley and Castro Limited-Length-Scale k-eps Model Revisited for Improved Performance in the Atmospheric Surface Layer Boundary-Layer Meteorol. 144 199–215

Troen I, Petersen EL (1989) European Wind Atlas. Risø National Laboratory, Roskilde. ISBN 87-550-1482-8, pp 656

Weng W, Taylor PA (2003) On Modelling the One-Dimensional Atmospheric Boundary Layer. Boundary –Layer Metorol., 107: 371-400

Wilby RL, Wigley TML (1997) Downscaling general circulation model output: a review of methods and limitations. Prog. Phys. Geog. 21: 530-548

Annex I: Model Descriptions

I.1. CFDWind

Managed by: Roberto Aurelio Chávez Arroyo, CENER

Description:

CFDWind is a family of micro-scale models developed in CENER and build on top the OpenFOAM CFD software (OpenFOAM, 2015). This family is currently composed of three versions considering different physical complexity levels.

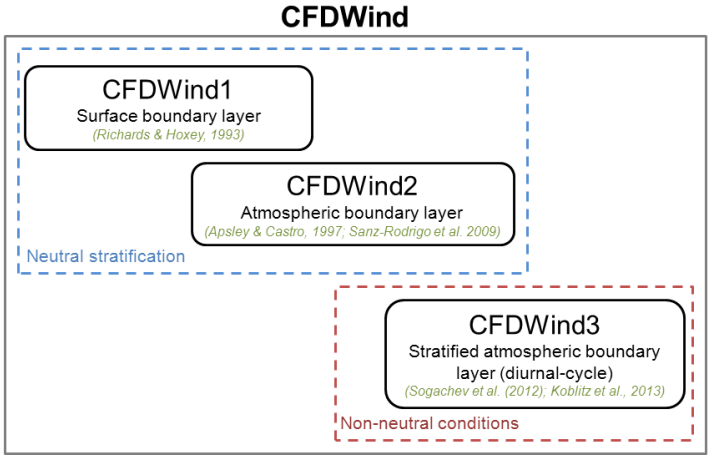

Figure I.1: Schematic diagram showing the naming convention, application and base publications describing the main physics of the CFDWind models

The three models are based on RANS/URANS equations for incompressible flows, in which turbulence closure is achieved using eddy-viscosity theory and two-equation closure schemes (k-ε, k-ω) modified for atmospheric flows.

As can be seen in the diagram above, the first two versions consider neutral stability and steady-state conditions while CFDWind3 is based on the Boussinesq approximation by including a buoyancy term together with the energy-transport equation in order to solve non-neutral atmospheric conditions.

More precisely, CFDWind1 deals with surface boundary layer (SBL) which complies with the Monin-Obukhov Similarity Theory (MOST) as proposed by Richards and Hoxey (1993) and Parente et al. (2011).

On the other hand, both v2 and v3 consider the whole Atmospheric Boundary Layer (ABL) structure by simulating the transition to geostrophic wind in the top boundary by adding the Coriolis force in the momentum equation as well as a length-scale limiter as proposed by Apsley and Castro (1997) for neutral conditions (CFDWind2) and further extended by Sogachev et al. (2012) and Koblitz et al. (2013) for non-neutral stratification (CFDWind3).

The coupling between pressure and velocity in the equations is solved by the well-known SIMPLE algorithm in case of the steady-state flows; whilst PISO algorithm is used to solve the coupling of the unsteady flows that emerge in the non-neutral cases.

When applied to any onshore non-flat site, all CFDWind models employ an automatic terrain mesh generator called *WindMesh*. This software was jointly developed by CENER and the Barcelona Supercomputing Center (BSC) specifically to generate structured terrain-following meshes that maximize the quality of mesh parameters such as orthogonality and skewness by applying certain angle filters and elliptic smoothing techniques.

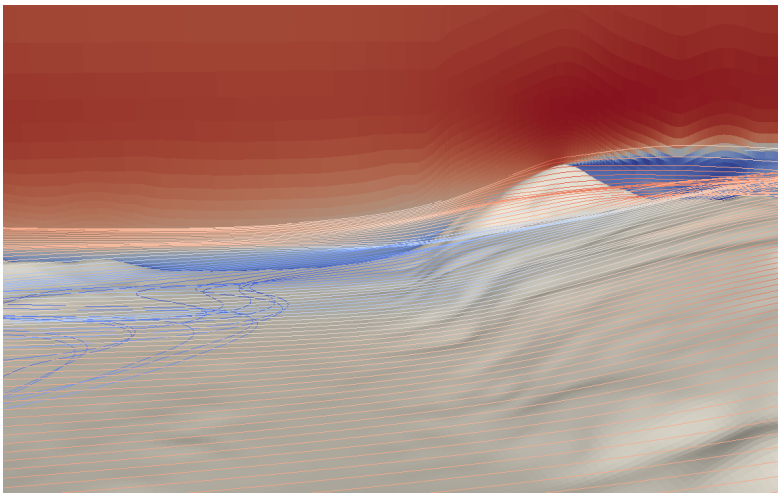

Figure I.2: Example of mean flow generated with CFDWind.

Different validation exercises of CFDWind1 and CFDWind2 can be found in Sanz-Rodrigo et al. (2011) and Chavez-Arroyo et al. (2014).

Solver: OpenFOAM

Software: In-house (will become open-source)

Regime: Steady

Main hypothesis: CFDWind 2.0 assumes isotropic eddy-viscosity turbulence, and the two-equation closure scheme (k-ε) modified for atmospheric flows. However, in order to extend the surface layer limitations to the full Atmospheric Boundary Layer (ABL) depth, it is necessary to include Coriolis effects and to limit the growth of turbulence with height, as demonstrated by Detering & Etling (1985).

This is achieved in the k-ε by adopting the Apsley & Castro (1994) correction on the Cε1 constant for neutral conditions.

A simulation of horizontally homogeneous conditions (i.e. a 1D) is firstly carried out as a precursor simulation in order to define the inlet conditions for the real-terrain run.

Turbulence closure: RANS eddy-viscosity

Turbulence model: k-ε modified through the Apsley and Castro (1997) approach.

ABL range: Atmospheric boundary layer (ABL)

Coriolis: yes

Atmospheric stability: no

Stability model: Under development, based on buoyancy source terms in the k-ε equations (Sogachev et al. 2012 and Koblitz et al. 2013)

Forest canopy: yes

Canopy model: Source/sink terms in the momentum and turbulence-closure equations as developed by Sogachev & Panferov (2006) and Sogachev (2009)

Wind turbine: yes

Rotor model : Actuator disk

Wake model: RANS Elliptic

Wind Farm Range: Multiple wake

Wake model additional information: Wakes have been always simulated with CFDWind 1.0 surface-layer model using actuator disk approach and several turbulence models (Cabezón et al., 2009). Simulation in the ABL solver of CFDWind 2.0 is possible but has not yet done.

Mesoscale coupling: no

Type of coupling: Statistical

Coupling additional information: coupling to mesoscale is under development, introducing mesoscale tendencies and baroclinicity as source terms in the momentum equations.

Remarks: Current development activities are devoted to introducing stability in the ABL model following Sogachev et al. (2012) and introducing mesoscale forcing with source terms. The precursor 1D model is used to generate cyclic diurnal cycles characteristic of the mean flow in horizontally-homogeneous conditions at varying surface stability and mesoscale forcing. The precursor is also used to remove surface drag from the mesoscale model in order to generalize the ABL forcing before introducing microscale effects.

CFDWind will be released open-source as part of the NEWA model-chain.

References:

Apsley D, Castro I (1997) A limited-length-scale k-ε model for the neutral and stably-stratified atmospheric boundary layer. Bound.-Lay. Meteorol. 83:75-78

Chávez-Arroyo R, Sanz-Rodrigo J, Gancarski P (2014) Modelling of atmospheric boundary-layer flow in complex terrain with different forest parameterizations. J. Physics: Conf. Series 524:012119

Koblitz T, Bechmann A, Sogachev A, Sørensen N, Réthoré P.E. (2013) Computational Fluid Dynamics model of stratified atmospheric boundary-layer flow. Wind Energy. online. DOI: 10.1002/we.1684

OpenFOAM (2015). OpenFOAM CFD Toolkit available at: http://www.openfoam.org/, last accessed October 2015

Parente A, Gorlé C, van Beeck J and Benocci C (2011) Improved k–ε model and wall function formulation for the RANS simulation of ABL flows. J. Wind Eng. Ind. Aerodyn. 99 267–278 ISSN 01676105

Richards PJ, Hoxey R (1993) Appropriate boundary conditions for computational wind engineering models using the k–ε turbulence model. J. Wind Eng. Ind. Aerodyn. 46-47: 145–153

Sanz-Rodrigo J, Cabezón D and García B. (2011) A systematic validation procedure for wind farm models in neutral atmospheric conditions. Proc. ICWE-13 Conf.

Sanz-Rodrigo J, Cabezón D, Lozano S, and Martí I (2009) Parameterization of the atmospheric boundary layer for offshore wind resource assessment with a limited-length-scale k-ε model. Proc. EWEA Conference.

Sogachev A, Panferov O (2006) Modification of two-equation models to account for plant drag. Bound.-Lay. Meteorol. 121: 229–266

Sogachev A (2009) A Note on Two-Equation Closure Modelling of Canopy Flow. Boundary Layer Meteorol. 130: 423-435

Sogachev A, Kelly M and Leclerc M. (2012) Consistent Two-Equation Closure Modelling for Atmospheric Research: Buoyancy and Vegetation Implementations. Bound.-Lay. Meteorol. 145:307–327

Webpage: http://it.cener.com/demo/windbench/models/cfdwind

I.2. Alya

Managed by: Matias Avila, Barcelona SuperComputing Center

Description:

Alya is a High Performance Computing multi-physics parallel solver based on finite elements and developed at Barcelona Supercomputing Center. Alya is able to run with tens of thousands of processors with an optimal scalability.

The model involves the solution of the Reynolds-Averaged Navier-Stokes (RANS) equations together with a k-ε turbulence model modified using a length-scale limiter, as initially proposed by Apsley and Castro (1997) to achieve a maximum mixing length in terms of Coriolis parameter. These equations are described in Avila et al. (2013).

Thermal and canopy models are implemented, based on Sogachev et al. (2012) and Koblitz et al. (2013).

The model involves automatic meshing and generation of initial and boundary conditions for atmospheric boundary layer. The automatic terrain mesh generator is called *WindMesh*. This software was jointly developed by the Barcelona Supercomputing Center (BSC) and CENER. It generates block structured terrain-following meshes that maximize the quality of the mesh by applying mesh optimization techniques described in Gargallo et al. (2015).

As the integration of the model up to the ground surface is still not viable for complex terrains, a specific law of the wall including roughness effects and based on Monin Obukhov equilibrium is implemented, (Richards and Hoxley, 1993; Koblitz et al. 2013).

The wake effects and the aerodynamic behavior of the wind turbines are described using the actuator disk model, that introduces a volumetric force in the momentum equations.

The equations mentioned previously are discretized in space using the finite element formulation based on the variational multiscale method, using linear interpolation for pressure, velocity and turbulence unknowns. The Navier Stokes equations are discretized using the algebraic subgrid scale model (ASGS), as described in Codina (2001). The k-ε equations are discretized using the finite element numerical scheme proposed by Codina and Soto (1999). A clipping limitation by below is applied to some terms of the differential equations as proposed by Lew and Buscaglia (2001).

The momentum and continuity equations are segregated solving the pressure Schur complement using the Orthomin iterative method described in Houzeaux et al. (2011). The momentum equation is solved implicitly using a GMRES solver. The continuity equation is solved with the Deflated Conjugate Gradient solver (DCG) (Lohner et al., 2011), together with an inlet preconditioner.

Solver: Alya

Software: In-house

Regime: Steady for neutral, Unsteady for thermal atmospheric stratification

Main hypothesis: Alya model assumes isotropic eddy-viscosity turbulence, and the two-equation closure scheme (k-ε) modified for atmospheric flows. However, in order to

extend the surface layer limitations to the full Atmospheric Boundary Layer (ABL) depth, it is necessary to include Coriolis effects and to limit the growth of turbulence with height, as demonstrated by Detering & Etling (1985). This is achieved in the k-ε model by adopting the Apsley & Castro (1997) correction on the C1 constant for neutral conditions.

A simulation of horizontally homogeneous conditions (i.e. a 1D) is firstly carried out as a precursor simulation in order to define the inlet conditions for the real-terrain run.

Turbulence closure: RANS eddy-viscosity

Turbulence model: k-ε modified through the Apsley and Castro (1997) approach.

ABL range: Atmospheric boundary layer (ABL)

Coriolis: yes

Atmospheric stability: yes

Stability model: Koblitz et al. 2013, Sogachev et al. (2012)

Forest canopy: yes

Canopy model: Sogachev et al. (2012)

Wind turbine: yes

Rotor model : Actuator disk

Wake model: RANS Elliptic

Wind Farm Range: Multiple wake

Mesoscale coupling: no

References:

Apsley D, Castro I (1997) A limited-length-scale k-ε model for the neutral and stably-stratified atmospheric boundary layer. Bound.-Lay. Meteorol. 83:75-78

Koblitz T, Bechmann A, Sogachev A, Sørensen N, Réthoré P.E. (2013) Computational Fluid Dynamics model of stratified atmospheric boundary-layer flow. Wind Energy. online. DOI: 10.1002/we.1684

Richards PJ, Hoxey R (1993) Appropriate boundary conditions for computational wind engineering models using the k–ε turbulence model. J. Wind Eng. Ind. Aerodyn. 46-47: 145–153

Sogachev A, Kelly M and Leclerc M. (2012) Consistent Two-Equation Closure Modelling for Atmospheric Research: Buoyancy and Vegetation Implementations. Bound.-Lay. Meteorol. 145:307–327

Codina R. (2001). A stabilized finite element method for generalized stationary incompressible flows, Computer Methods in Applied Mechanics and Engineering 190, (20–21) 2681–2706.

Codina R., Soto O. (1999). Finite element implementation of two-equation and algebraic stress turbulence models for steady incompressible flows, IJNMF 30,309–334.

Avila M., Folch A., Houzeaux G., Eguzkitza B., Prieto L., Cabezón D.. (2013) A Parallel CFD Model for Wind Farms; Procedia Computer Science, Volume 18, Pages 2157-2166.

Lew A., Buscaglia G., and Carrica P.M. (2001). A note on the numerical treatment of the k-epsilon turbulence model. International Journal of Computational Fluid Dynamics, 14(3):201-209

Houzeaux G, Aubry R, Vázquez M - Computers & Fluids (2011). Extension of fractional step techniques for incompressible flows: The preconditioned Orthomin (1) for the pressure Schur complement. Computers & Fluis 44, 297-313

Gargallo-Peiró A., Avila M., Owen H., Prieto L., Folch A.,(2015) Mesh Generation for Atmospheric Boundary Layer Simulation in Wind Farm Design and Management, Procedia Engineering 124, Pages 239-251

Löhner R., Mut F., Cebral J. R., Aubry R. and Houzeaux G. (2011), Deflated preconditioned conjugate gradient solvers for the pressure-Poisson equation: Extensions and improvements. Int. J. Numer. Meth. Engng., 87: 2–14.

I.3. ArgoDG

Managed by: Koen Hillewaert, Cenaero

Description:

Cenaero is developing a high order code (Argo DG) which has shown promising results in terms of accuracy and scalability on LES of low Reynolds number flows over smooth surfaces. In parallel to the NEWA project, Cenaero is developing wall models in order to perform LES of high Reynolds number flows over rough walls.

DGM is a finite element discretization that features high order of accuracy on unstructured meshes, low dissipation, massive parallelism and geometrical flexibility. The method can be seen as a collection of element-wise defined small finite element problems, coupled across the element interfaces by weak Dirichlet "boundary" conditions. The high order of convergence is then ensured by the cell-wise independent polynomial interpolation in each cell, as illustrated in the figure below.

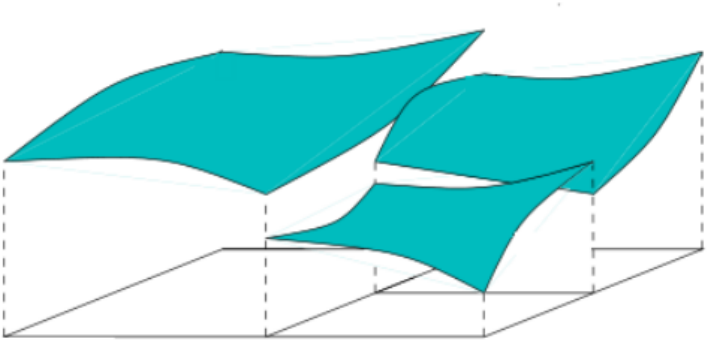

Figure I.3: Artists impression of a discontinuous interpolant, typical for the Discontinuous Galerkin Method.

Solver: ArgoDG

Software: In-house

Regime: Unsteady

Turbulence closure: Large Eddy Simulation (LES)

Turbulence model: Implicit LES (ILES) where the subgrid scale stresses are provided by the numerical scheme.

ABL range: Surface layer (SL)

Coriolis: no

Atmospheric stability: no

Forest canopy: no

Wind turbine: no

Mesoscale coupling: no

Remarks: The code Argo has previously been successfully validated and assessed on DNS and ILES of academic benchmarks such as the DNS of transition of the Taylor-Green vortex and ILES of homogeneous isotropic turbulence and channel flow, thereby demonstrating similar accuracy as dedicated academic codes. The code is already being applied to DNS of industrial benchmarks featuring transitional flow.

The development of wall models should be finished during the third year of the NEWA project and Cenaero could then offer to use Argo DG code to perform LES of some large test cases (via a PRACE project). The use of Argo DG in the NEWA project is hence not certain at this stage; it will depend on Cenaero's development and on the future project needs.

References:

Hillewaert, K. (2013) Development of the Discontinuous Galerkin Method for high-resolution, large scale CFD and acoustics in industrial geometries, Ph.D. thesis, Institute of Mechanics, Materials and Civil Engineering, Ecole polytechnique de Louvain, Louvain-la-Neuve, Belgium.

Carton de Wiart, C. (2014) Towards a discontinuous Galerkin solver for scale-resolving simulations of moderate Reynolds number flows, and application to industrial cases, Ph.D. thesis, Institute of Mechanics, Materials and Civil Engineering, Ecole polytechnique de Louvain, Louvain-la-Neuve, Belgium.

Carton de Wiart, C., Hillewaert, K., Duponcheel, M., and Winckelmans, G. (2014) Assessment of a discontinuous Galerkin method for the simulation of vortical flows at high Reynolds number, International Journal for Numerical Methods in Fluids, Vol. 74, No. 7, pp. 469–493, doi: 10.1002/fld.3859.

Carton de Wiart, C., Hillewaert, K., Bricteux, L., and Winckelmans, G., LES using a Discontinuous Galerkin Method: isotropic turbulence, channel flow and periodic flow, Proceedings of the ERCOFTAC Workshop. Direct and Large-Eddy Simulation 9, ERCOFTAC, Dresden, Germany, April 3-5.

Carton de Wiart, C. and Hillewaert, K. (2012) DNS and ILES of transitional flows around a SD7003 airfoil using a high order Discontinuous Galerkin Method (paper ICCFD7-2012-3604), Seventh International Conference on Computational Fluid Dynamics, Hawai, USA.

A.Frère, K. Hillewaert, H. Sarlak, and R. F. Mikkelsen (2015) Cross-Validation of Numerical and Experimental Studies of Transitional Airfoil Performance », 33rd Wind Energy Symposium, 5-9, Kissimmee, Florida.

Hillewaert, K., Carton de Wiart, C., Verheylewegen, G., and Arts, T. (2014) Assessment of a high-order discontinuous Galerkin method for the direct numerical simulation of transition at low Reynolds number in the T106C high-lift low pressure turbine cascade, Proceedings of the ASME Turbine Technical Conference and Exhibition, No. GT2014-26739, ASME Turbo Expo.

I.4. IWES RANS

Managed by: Chi-Yao Chang, Fraunhofer IWES

Description:

IWES RANS is a CFD model based on OpenFOAM adapted for the wind flow modeling over terrain. It can be used to simulate both the surface boundary layer and the atmospheric boundary layer by enabling the Coriolis force and mixing-length limitation.

In both usages (SBL and ABL) it uses as inlet precursor 1D velocity and turbulent profiles in order to get a consistency with the turbulence model. This methodology can avoid certain degree of numerical errors.

The 3D mesh is generated by an in-house open source tool called terrainBlockMesher (www.github.com/jonasIWES/terrainBlockMesher) for meshing complex terrain. This tool is based on OF's blockMesh system and it creates a generalized blockMeshDict using splines which can then be read by blockMesh.

The procedure creates a structured mesh from STL-data whose inputs are the number of blocks and cells in X,Y,Z, grading, plus some parameters for mesh refinement and softening the terrain in the far field.

Solver: OpenFOAM

Software: In-house

Regime: Steady

Main hypothesis: Steady state solver based on OpenFOAM's simpleFoam (version 2.1.1). Isotropic eddy-viscosity turbulence using the Boussinesq approximation.

Turbulence closure: RANS eddy-viscosity

Turbulence model: k-ε modified through the Apsley and Castro (1997) approach.

ABL range: Atmospheric boundary layer (ABL)

Coriolis: yes

Atmospheric stability: no

Forest canopy: yes

Canopy model: Source terms in momentum equations (Crasto 2007)

Wind turbine: yes

Rotor model : Actuator disk

Wake model: RANS Elliptic

Wind Farm Range: Multiple wake

Mesoscale coupling: no

Remarks: Stability model and additional forest canopy models are under development and will be implemented during the NEWA project.

In addition to the contribution to the open source microscale reference model developed within the NEWA, the software terrainBlockMesher will be released open-source at the end of the project.

Besides Franhoufer IWES, this model has been also applied by Cenaero as part of the benchmarking exercise for the sensitivity analysis in the Kassel test site.

Despite that Cenaero is not planning to do any particular OpenFOAM-based development, it is their aim to investigate the capabilities of current (and further coming following the developments within NEWA) OpenFOAM-based solvers in order to contribute to provide a reliable open-source tool to the end-user by the end of the NEWA project.

References:

Crasto, G. (2007). PhD Thesis. Universita degli Studi di Cagliari.

Richards P.J., Hoxey R. (1993) Appropriate boundary conditions for computational wind engineering models using the k–ε turbulence model, J. Wind Eng. Ind. Aerodyn. 46-47: 145–153

Schmidt, J., Peralta, C., & Stoevesandt, B. (2012). Automated generation of structured meshes for wind energy applications. In Open Source CFD International Conference. London.

I.5. PALM

Managed by: Björn Witha, ForWind, University of Oldenburg

Description:

PALM (Maronga et al., 2015; Raasch et al., 2001) is a large-eddy simulation (LES) model for atmospheric and oceanic flows which is especially designed for performing on massively parallel computer architectures. PALM is free software. It can be redistributed and/or modified under the terms of the GNU General Public License (v3).

PALM has been widely used in the field of boundary-layer meteorology during the last 15 years. Since 2009, it has been applied to simulate the wake of single wind turbines and wind farms. PALM runs currently on machines of all leading manufacturers of supercomputers. As it is possible to carry out simulations on huge numbers of cores (so far tested up to 32000), a huge number of grid points (up to 10 to the power of 10) can be used. For details on PALM see the PALM homepage: https://palm.muk.uni-hannover.de.

Some of PALM's highlights are:

- excellent scaling, so far tested up to 32000 cores
- online data analysis (during model runs) in order to avoid I/O bottlenecks
- topography realized on cartesian grid (allows for steep topography)
- non-cyclic horizontal boundary conditions including turbulent inflow
- large-scale forcing and nudging with measurements or mesoscale model
- wind turbine model (to be included in default code soon)
- full land surface model
- code can be switched to ocean version with salinity equation and equation of state for seawater
- embedded parallelized Lagrangian particle model for various applications (footprint calculation, simulation of cloud droplet growth, visualization, etc.)
- interface which allows users to plug in their own code extensions without modifying the default code
- advanced shell scripts for installing and running the code in interactive and batch mode are available
- code is permanently maintained and improved by the PALM group and other users; code management is based on subversion

Solver: CFD, LES for incompressible 3D turbulent ABL flow

Software: Open-source

Regime: Unsteady

Main hypothesis: PALM explicitly solves the boussinesq-approximated, filtered Navier-Stokes equations, the subgrid-scale turbulence is modeled.

Turbulence closure: Large Eddy Simulation (LES)

Turbulence model: Subgrid-scale turbulence: 1.5th order closure Smagorinsky model with the modifications by Deardorff (1980); large-scale turbulence is explicitly resolved.

ABL range: Atmospheric boundary layer (ABL)

Coriolis: yes

Atmospheric stability: yes

> **Stability model**: The desired stability can be prescribed as boundary condition (temperature gradient, surface heat flux). Between the surface and the first grid level Monin-Obukhov theory and the Dyer-Businger functions are applied.

Forest canopy: yes

> **Canopy model**: Plant canopy model of Watanabe (2004).

Wind turbine: yes

> **Rotor model** : Actuator disk with rotation, actuator disk, actuator line
>
> **Wake model**: Large-Eddy Simulation (LES)
>
> **Wind Farm Range**: Multiple wake
>
> **Wake model additional information**: Two actuator disk models are available: a standard uniform loaded disk and an enhanced model with non-uniform loading and rotation after Wu and Porté-Agel (2011). Tower and nacelle parameterizations are included as well. An actuator line model is also available (but due to the high computational cost only suited for single wake simulations)

Mesoscale coupling: yes

> **Type of coupling**: Dynamic
>
> **Coupling additional information**: Large-scale forcing with mesoscale simulation output (WRF) and nudging, it is only a one-way coupling

Remarks: The large-scaling forcing and nudging will be further tested within NEWA and probably modified. PALM will not be part of the NEWA model chain but used for verification and validation with the other microscale models. Furthermore, PALM simulations are planned for the support of the experiments in Perdigao and Kassel and to investigate further idealized test cases like the transition of the flow from land to sea (validation with data from the RUNE experiment) and probably the diurnal cycle.

Although not relevant for NEWA, the wind turbine model is currently implemented in the default code. During the course of the project, PALM is planned to be further enhanced by the developers, e.g. with a different subgrid scale model and viscous (instead of rastered) topography.

References:

Maronga, B., M. Gryschka, R. Heinze, F. Hoffmann, F. Kanani-Sühring, M. Keck, K. Ketelsen, M. O. Letzel, M. Sühring, S. Raasch (2015): The Parallelized Large-Eddy

Simulation Model (PALM) version 4.0 for atmospheric and oceanic flows: model formulation, recent developments, and future perspectives, *Geosci. Model Dev.*, **8**, 2515-2551

Raasch, S., M. Schröter (2001): PALM – A large-eddy simulation model performing on massively parallel computers, *Meteorol. Z.*, **10**, 363-372

Deardorff, J. W. (1980): Stratocumulus-capped mixed layers derived from a three-dimensional model, *Boundary-Layer Meteorol.*, **18**, 495-527

Watanabe, T. (2004): Large-Eddy Simulation of Coherent Turbulence Structures Associated With Scalar Ramps Over Plant Canopies, *Boundary-Layer Meteorol.*, **112**, 307–341

Wu, Y.-T., F. Porté-Agel (2011): Large-Eddy Simulation of Wind-Turbine Wakes: Evaluation of Turbine Parametrisations, *Boundary-Layer Meteorol.*, **138**, 345-366

Webpage: https://palm.muk.uni-hannover.de

I.6. EllipSys3D-ABL (WAsP CFD)

Managed by: Andreas Bechmann, DTU

Description:

The EllipSys3D code (Sørensen, 1995; Michelsen, 1992; 1994) is a general-purpose flow solver used for many applications within wind energy. EllipSys3Dis a multiblock finite-volume discretization of the incompressible Navier-Stoke equations in general curvilinear coordinates.

The user can choose among different discretization schemes for the convective terms, all implemented using the deferred correction approach first suggested by Khosla and Rubin (1974). WAsP-CFD uses a third order scheme (QUICK) to retain high accuracy. Central differences are used for the remaining terms of the Navier-Stokes equations.

EllipSys3D is parallelized with MPI for execution on distributed memory machines, using a non-overlapping domain decomposition technique and uses a multi-level grid sequence in steady-state computations to further accelerate computations. The parallelization allows for an efficient use of large computer clusters and consequently calculations on large, high-resolution grids, but the multi-level grid sequence has the added benefit of automatically making a grid independence test since EllipSys3D produces a result on each of the differently resolved grid levels.

The code uses a collocated variable arrangement, and Rhie and Chow (1982) interpolation is used to avoid odd/even pressure decoupling. The solution is advanced in time using a 2nd order iterative time-stepping (or dual time-stepping) method. In each global time-step the equations are solved in an iterative manner, using under-relaxation. First, the momentum equations are used as a predictor to advance the solution in time. At this point in the computation the flow field will not fulfil the continuity equation. The rewritten continuity equation (the so called pressure correction equation) is used as a corrector making the predicted flow field satisfy the continuity constraint. This two-step procedure corresponds to a single sub-iteration, and the process is repeated until a convergent solution is obtained for the time-step. When a convergent solution is obtained, the variables are updated, and we continue with the next time-step.

The three momentum equations are solved decoupled using a red/black Gauss-Seidel point solver. The solution of the Poisson system arising from the pressure correction equation is accelerated using a multigrid method. In order to accelerate the overall algorithm, a three level grid sequence and local time stepping are used.

Solver: EllipSys3D

Software: In-house

Regime: Unsteady

Main hypothesis: Isotropic eddy-viscosity turbulence, and the two-equation closure scheme (k-ε) modified for atmospheric flows. However, in order to extend the surface

layer limitations to the full Atmospheric Boundary Layer (ABL) depth, it is necessary to include Coriolis effects and to limit the growth of turbulence with height, as demonstrated by Detering & Etling (1985).

This is achieved in the k-ε by adopting the Apsley & Castro (1994) correction on the Cε1 constant for neutral conditions.

A simulation of horizontally homogeneous conditions (i.e. a 1D) is firstly carried out as a precursor simulation in order to define the inlet conditions for the real-terrain run.

Turbulence closure: RANS eddy-viscosity

Turbulence model: k-ε modified through the Apsley and Castro (1997) approach.

ABL range: Atmospheric boundary layer (ABL)

Coriolis: yes

Atmospheric stability: yes

> **Stability model**: Diurnal cycle based on buoyancy source terms in the k-ε equations (Sogachev et al. 2012 and Koblitz et al. 2013)

Forest canopy: yes

> **Canopy model**: Source/sink terms in the momentum and turbulence-closure equations as developed by Sogachev & Panferov (2006) and Sogachev (2009)

Wind turbine: no

Mesoscale coupling: yes

> **Type of coupling**: Statistical
>
> **Coupling additional information**: coupling to mesoscale is under development through the “generalized wind” concept (Troen et al., 2014)

Remarks: Based on model-chain methodology that will be developed in the NEWA project, the EllipSys3D code is planned to be used to generate (one of the) layers of the wind velocity at microscale level covering the whole European domain.

References:

Apsley D, Castro I (1997) A limited-length-scale k-ε model for the neutral and stably-stratified atmospheric boundary layer. Bound.-Lay. Meteorol. 83:75-78

Koblitz T, Bechmann A, Sogachev A, Sørensen N, Réthoré P.E. (2013) Computational Fluid Dynamics model of stratified atmospheric boundary-layer flow. Wind Energy. online. DOI: 10.1002/we.1684

Michelsen J.A.(1992) Basis3D - a Platform for Development of Multiblock PDE Solvers.Technical Report AFM 92-05, Technical University of Denmark.

Michelsen J.A. (1994) Block structured Multigrid solution of 2D and 3D elliptic PDE's”, Technical Report AFM 94-06, Technical University of Denmark.

Rhie, C. and Chow, W. (1982) A numerical study of the turbulent flow past an isolated airfoil with trailing edge separation. In 3rd Joint Thermophysics, Fluids, Plasma and Heat

Transfer Conference, Fluid Dynamics and Colocated Conferences. American Institute of Aeronautics and Astronautics.

Sogachev A, Panferov O (2006) Modification of two-equation models to account for plant drag. Bound.-Lay. Meteorol. 121: 229–266

Sogachev A (2009) A Note on Two-Equation Closure Modelling of Canopy Flow. Boundary Layer Meteorol. 130: 423-435

Sogachev A, Kelly M and Leclerc M. (2012) Consistent Two-Equation Closure Modelling for Atmospheric Research: Buoyancy and Vegetation Implementations. Bound.-Lay. Meteorol. 145:307–327

Sørensen N.N. (1995) General Purpose Flow Solver Applied to Flow over Hills", Risø-R-827-(EN), Risø National Laboratory, Roskilde, Denmark.

Troen, I., Bechmann, A., Kelly, M. C., Sørensen, N. N., Réthoré, P-E., Cavar, D., & Ejsing Jørgensen, H. (2014) Complex terrain wind resource estimation with the wind-atlas method: Prediction errors using linearized and nonlinear CFD micro-scale models. Proceedings of EWEA 2014. European Wind Energy Association (EWEA).

Webpage: http://www.wasp.dk/waspcfd

Acknowledgements

The NEWA project counts with the support from an ERA-Net Plus consortium composed by the European Commission and 9 funding agencies from 8 member states:

- Public Service of Wallonia, Department of Energy and Sustainable Building (Belgium)
- Department of Economy, Science and Innovation Flemish Government (Belgium)
- Danish Energy Authority (Denmark)
- Federal Ministry for the Economic Affairs and Energy, on the basis of the decision by the German Bundestag (Germany)
- Latvijas Zinatnu Akademija (Latvia)
- Fundação para a Ciência e a Tecnologia (Portugal)
- Ministerio de Economía y Competitividad (Spain)
- The Swedish Energy Agency (Sweden)
- The Scientific and Technological Research Council of Turkey (Turkey)